R-13-15

The corrosion rate of copper in a bentonite test package measured with electric resistance sensors

Bo Rosborg, Division of Surface and Corrosion Science, KTH

Tadeja Kosec, Andrej Kranjc, Viljem Kuhar, Andraz Legat
Slovenian National Building and Civil Engineering Institute

December 2012

Svensk Kärnbränslehantering AB
Swedish Nuclear Fuel
and Waste Management Co

Box 250, SE-101 24 Stockholm
Phone +46 8 459 84 00

ISSN 1402-3091
SKB R-13-15
ID 1369602

The corrosion rate of copper in a bentonite test package measured with electric resistance sensors

Bo Rosborg, Division of Surface and Corrosion Science, KTH

Tadeja Kosec, Andrej Kranjc, Viljem Kuhar, Andraz Legat
Slovenian National Building and Civil Engineering Institute

December 2012

Keywords: Bentonite clay, Corrosion rate, Electric resistance sensors, Electrochemical measurements, Long-term exposure, Oxic conditions, Pure copper, Saline groundwater.

Abstract

LOT[1] test parcel A2 was exposed for six years in the Äspö Hard Rock Laboratory, which offers a realistic environment for the conditions that will prevail in a deep repository for high-level radioactive waste disposal in Sweden. The test parcel contained copper electrodes for real-time corrosion monitoring in bentonite ring 36, where the temperature was 24°C, and copper coupons in bentonite rings 22 and 30, where the temperature was higher. After retrieval of the test parcel in January 2006, a bentonite test package consisting of bentonite rings 35–37 was placed in a container and sealed with a thick layer of paraffin. Later the same year new copper electrodes were installed in the test package.

In January 2007 electric resistance (ER) sensors of pure copper with a thickness of 35 µm were also installed in the test package mainly to facilitate the interpretation of the results from the real-time corrosion monitoring with electrochemical techniques. The results from the ER measurements performed at room temperature from start of exposure in January 2007 up to the end of exposure in April 2011 are presented in this report together with back-up information from electrochemical measurements and the post-test examination of the ER sensors and retrieved copper coupons.

The ER sensors have with time obtained somewhat higher corrosion potentials than the pre-exposed and the new copper electrodes with all revealing oxic conditions in the test package; the corrosion potential of the ER sensors fell in the range 222–261 mV (SHE) in the end of exposure. Two out of four ER sensors survived all through the four years exposure. One sensor failed quite early, and another failed late in the exposure. The *recorded* corrosion rate for the latter was significantly higher than for the two survivors; for instance almost 7 compared to less than 1.5 µm/year after three years exposure. It was anticipated that the failed sensors had experienced an uneven corrosion attack, which was also revealed by the post-test examination. The corrosion attack on the exposed sensor elements varied from only a slight attack to full penetration of the 35 µm thick sensor lead. The *recorded* corrosion rate of the sensors at the start of exposure in the test package was higher than 15 µm/year and the *recorded* corrosion rate on the two survivors in the end of the four years exposure was 0.7 and 0.8 µm/year. From electrochemical impedance spectroscopy (EIS) the corrosion rates for the four sensors in the end of exposure were estimated to 0.3, 1.1, 0.5, and 0.5 µm/year respectively. By comparing cross-sections from corroded and protected (reference) sensor elements from the very same ER sensor, the average corrosion rates for the four sensors during the 1,539 days of exposure were estimated to 2.0, 2.9, 2.7, and 1.6 µm/year respectively.

The ER measurements have shown that the corrosion rate of pure copper exposed in an oxic bentonite/saline groundwater environment at room temperate decreases slowly with time to low but measurable values. The corrosion rates estimated from the regularly performed EIS measurements replicate the ER data. Thus, for this oxic environment in which copper acquires corrosion potentials of the order of 200 mV (SHE) or higher, electrochemical measurements provide believable data. Comparing the *recorded* ER data with an estimate of the average corrosion rate based on comparing cross-sections from exposed and protected sensor elements, it is obvious that the former overestimates the actual corrosion rate, which is understandable. It seems as if electrochemical measurements can provide a better estimate of the corrosion rate; however, this is quite dependent on the use of proper measuring frequencies and evaluation methods. In this respect ER measurements are more reliable.

It has been shown that real-time[2] corrosion monitoring by electrochemical and ER techniques can be used to follow the corrosion rate of copper in oxic bentonite/saline groundwater environments (alike the used environmental conditions; for other redox conditions the situation could be different). The post-test examination of the four ER sensors after a test period of 1,539 days revealed cuprite and paratacamite as end corrosion products, uneven corrosion on the copper leads, and average corrosion rates below 3 µm/year similar to what has been found for copper coupons exposed in the LOT test parcels at Äspö.

[1] Acronym for the project "Long Term Test of Buffer Material" at the Äspö Hard Rock Laboratory.

[2] Strictly, neither the ER nor the EIS measurements are true real-time measurements, however, considering the long exposure times in this case they serve as such.

Sammanfattning

LOT-projektets[3] försökspaket A2 exponerades under sex år i Äspölaboratoriet, som erbjuder en realistisk miljö vad gäller förhållandena i ett djupförvar för högaktivt nukleärt avfall i Sverige. Försökspaketet innehöll kopparelektroder i bentonitringen 36 för korrosionsmonitering i realtid, i vilken temperaturen var 24°C, och kopparkuponger i bentonitringarna 22 and 30, där temperaturen var högre. Efter upptaget av försökspaketet i januari 2006, placerades ett testpaket bestående av bentonitringarna 35–37 i en behållare och göts in i ett tjockt lager paraffin. Senare under året installerades nya kopparelektroder i testpaketet.

I januari 2007 installerades elektrisk resistans (ER)-givare av ren koppar och tjockleken 35 µm i testpaketet, främst för att understödja tolkningen av utförd korrosionsmonitering med elektrokemiska metoder. Resultaten från de vid rumstemperatur utförda ER-mätningarna från start av exponeringen i januari 2007 fram till april 2011 presenteras i denna rapport tillsammans med kompletterande information från utförda elektrokemiska mätningar och efterundersökningen av ER-givarna och upptagna kopparkuponger.

ER-givarna har med tiden uppnått något högre korrosionspotential jämfört med de förexponerade och nyinsatta kopparelektroderna, med samtliga visande på oxiderande förhållanden i testpaketet; korrosionspotentialen för ER-givarna låg inom intervallet 222–261 mV (SHE) i slutet av exponeringen. Två av fyra ER-givare överlevde de fyra årens exponering. En givare slutade fungera relativt tidigt och en annan sent under exponeringen. *Uppmätt* korrosionshastighet för den senare var betydligt högre än för de två som hela tiden fungerade; exempelvis var korrosionshastigheten nära 7 jämfört med mindre än 1,5 µm/år efter tre års exponering. De havererade givarna förväntades ha undergått en ojämn korrosion under exponeringen, vilket också efterundersökningen bekräftade. Korrosionen på de exponerade givarelementen varierade från nära nog ingen korrosion till fullständig korrosion av den 35 µm tjocka elledaren. Korrosionshastigheten vid start av exponeringen var högre än 15 µm/år och *uppmätt* korrosionshastighet efter fyra års exponering var 0,7 och 0,8 µm/år för de fungerande givarna. Med hjälp av elektrokemisk impedansspektroskopi (EIS) uppskattades korrosionshastigheten för de fyra givarna i slutet av exponeringen till 0,3, 1,1, 0,5, respektive 0,5 µm/år. Genom att jämföra tvärsnitt på korroderade och skyddade (referens-) givarelement från en och samma ER-givare uppskattades den genomsnittliga korrosionshastigheten på de fyra givarna under 1 539 dagars exponering till 2,0, 2,9, 2,7, respektive 1,6 µm/år.

ER-mätningarna har visat att korrosionshastigheten för ren koppar exponerad i en bentonit/salt grundvatten-miljö vid rumstemperatur med tiden sakta sjunker till låga men mätbara nivåer. De korrosionshastigheter som erhållits från regelbundet utförda EIS-mätningar följer uppmätta ER-data. För använd oxiderande miljö, i vilken koppar erhåller korrosionspotentialer på 200 mV (SHE) eller högre, ger alltså de elektrokemiska mätningarna trovärdiga resultat. Jämförs uppmätta ER-data med uppskattad genomsnittlig korrosionshastighet baserad på uppmätta tvärsnitt på exponerade och skyddade givarelement så är det uppenbart att de förra överskattar den verkliga korrosionshastigheten, vilket är förståeligt. De elektrokemiska mätningarna tycks kunna uppskatta korrosionshastigheten bättre, men en förutsättning är att en adekvat mätfrekvens och utvärdering används. Av denna anledning kan ER-mätningar vara mer pålitliga.

Det har visats att såväl elektrokemiska mätningar som ER-mätningar kan användas för att i realtid[4] följa korrosionshastigheten på koppar i bentonit/salt grundvatten-miljö åtminstone under oxiderande förhållanden (motsvarande den miljö som här använts; för andra redox-förhållanden kan det vara annorlunda). Efterundersökningen av de fyra ER-sensorerna efter 1 539 dagars exponering uppvisade korrosionsprodukterna kuprit och paratakamit på kopparledarna, ojämn korrosion på desamma, och genomsnittliga korrosionshastigheter under 3 µm/år liknande vad som efterundersökningarna av kopparkupongerna från LOT-projektets testpaket visat.

[3] Akronym för projektet "Long Term Test of Buffer Material" vid Äspölaboratoriet.

[4] Även om vare sig ER- eller EIS-mätningar i strikt bemärkelse är egentliga realtidsmätningar så kan de här betraktas som sådana med tanke på de långa exponeringstiderna.

Acknowledgements

Christina Lilja and Lars Werme (formerly of SKB) at the SKB head office in Stockholm are gratefully acknowledged for their support. So are Ulf Nilsson at Clay Technology AB for help with cutting of the bentonite test package, Monika Prosenc at the Slovenian National Building and Civil Engineering Institute for the cross-section microscopy, Anastasia Riazanova at the Royal Institute of Technology in Stockholm for the dual beam electron microscopy, and Srečo Škapin at the Jožef Stefan Institute in Ljubljana for the XRD analysis.

Contents

1 Background

The principal strategy for high-level radioactive waste disposal in Sweden is to enclose the spent nuclear fuel in tightly sealed copper canisters that are embedded in bentonite clay about 500 m down in the Swedish bed-rock (Figure 1-1) (Rosborg and Werme 2008). The repository will be built using materials that occur naturally in the earth's crust. The idea is that the repository should imitate nature as closely as possible.

"Nature" has proven (i) that copper can last many millions of years under proper conditions – native copper has been preserved for nearly 200 million years in an environment which is similar to the repository near-field environment, (ii) that bentonite clay has existed for many million years – Wyoming bentonite clay for instance was formed during the Cretaceous period, i.e. more than 65 million years ago, and (iii) that the Fennoscandian bedrock shield is stable – the bedrock of interest was formed during the Precambrian period, i.e. more than 545 million years ago.

Besides rock movement, the biggest threat to the copper canister in the repository is corrosion. It is believed that copper will last indefinitely if proper environmental conditions are established and maintained. The most important task from a corrosion point of view is to ascertain a proper near-field environment for the copper canister.

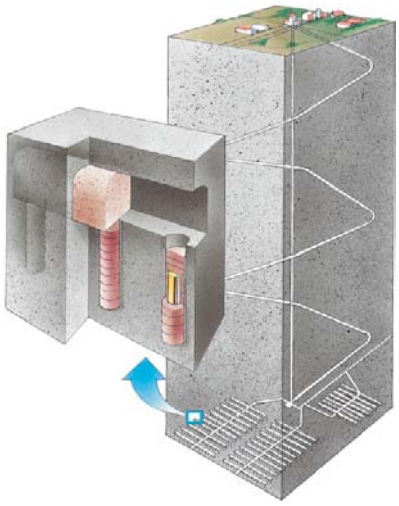

Figure 1-1. *Illustration of a repository for high-level radioactive waste disposal according to the Swedish KBS-3 design.*

2 The material-environment system

Here information about the copper material, the saline groundwater, the bentonite clay, and the near-field environment is presented with the dual purpose of describing the anticipated conditions in a deep repository for high-level radioactive waste disposal in Sweden, and the actual test conditions for the copper samples used in the present study.

Cylindrical electrodes and rectangular coupons of pure copper have been exposed for six years in LOT test parcel A2 at a depth of 450 m in the Äspö Hard Rock Laboratory (HRL) (Figure 2-1a) (Karnland et al. 2009). The laboratory offers a realistic environment for different experiments and tests under the conditions that will prevail in a deep repository. The cylindrical electrodes were exposed in bentonite ring 36 of the test parcel and the coupons in bentonite rings 22 and 30 (Figure 2-1b). The former were included for real-time corrosion monitoring (a pilot effort) and the coupons were included to gain information about the nature and extent of the corrosion.

2.1 The copper material

The copper canisters are manufactured from pure oxygen-free copper (99.99% Cu) with a deliberate addition of approximately 50 ppm phosphorous to improve creep properties (Werme 1998). The cylindrical copper electrodes and rectangular coupons used in the present work were manufactured from actual canister material.

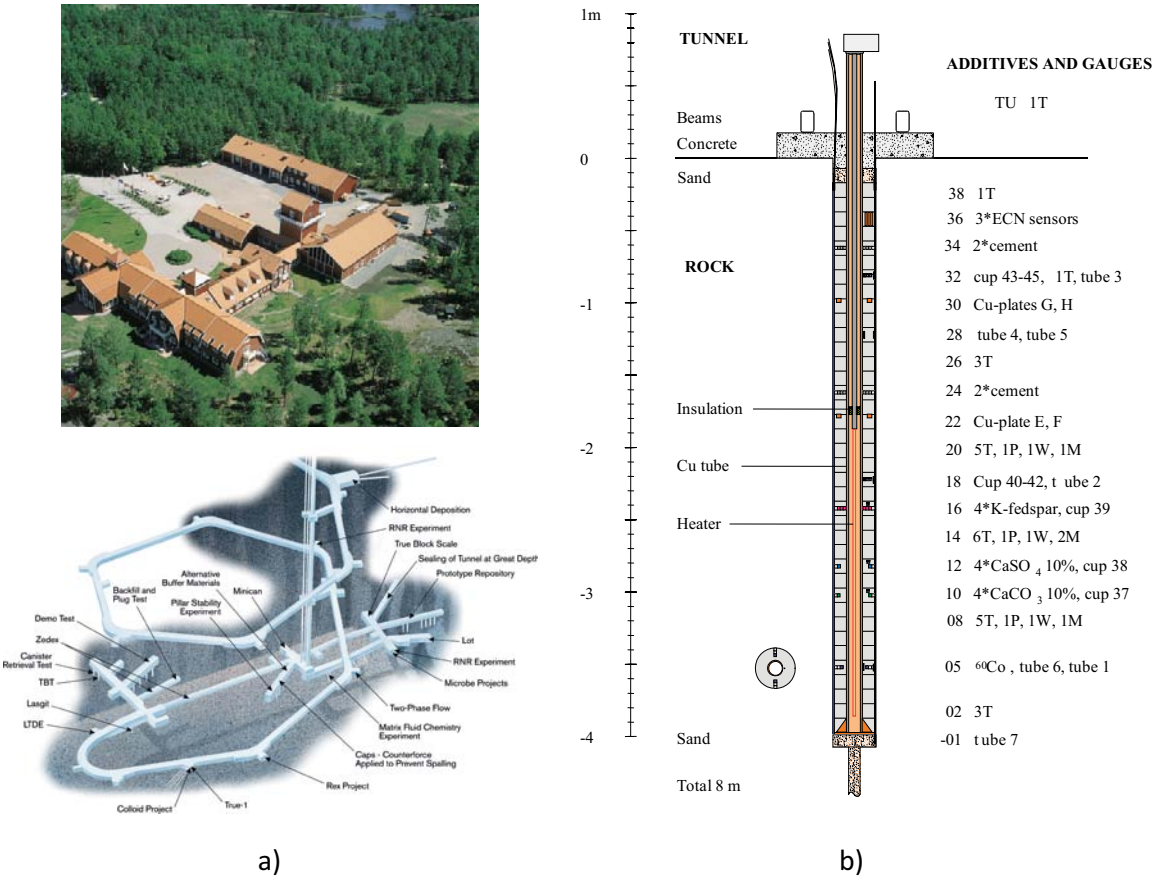

a) b)

Figure 2-1. *(a) View of the Äspö Hard Rock Laboratory above and below ground, and (b) LOT test parcel A2 exposed for six years in the laboratory. The cylindrical copper electrodes were positioned in bentonite ring 36 (24°C) and the copper coupons in bentonite rings 22 (75°C) and 30 (30°C).*

2.2 The saline groundwater

Groundwater in granitic rock in Sweden is oxygen-free and reducing below a depth of 100 to 200 m. The redox potential below this depth ranges between –200 and –350 mV (SHE) and the water has a pH ranging from neutral to mildly alkaline (pH 7–9) (King et al. 2001, 2010). The chloride concentration in the groundwater can vary within very wide limits, from 5 mg/dm^3 to 50 g/dm^3. Groundwater analyses from different parts of Sweden show sulphide concentrations ranging from < 0.01 mg/dm^3 up to 1 mg/dm^3, with 0.1 mg/dm^3 as a typical value. Dissolving sulphide minerals are one source of sulphide in the groundwater, but sulphide will also be produced by a specific group of micro organisms, the sulphate-reducing bacteria, which are common in deep groundwater.

Table 2-1 shows the composition of the groundwater at the test position for LOT test parcel A2 in the Äspö HRL.

2.3 The bentonite clay

The main mineral constituent in bentonite clay is montmorillonite, which has a sheet-like crystal structure (Karnland et al. 2006). As an example, Wyoming bentonite used in this study, and sold under the commercial name MX-80, is dominated by natural sodium montmorillonite clay (~80% by weight), which is responsible for the desired physical properties. Accessory minerals are quartz (~4%), tridymite (~4%), cristobalite (~3%), feldspars (~4%), muscovite/illite (~4%), sulphides (~0.2%), and small amounts of other minerals and organic carbon (~0.4%). The mean mineralogical composition of the montmorillonite is given by:

$(Al_{3.10}\ Fe^{3+}_{0.4}\ Fe^{2+}_{0.02}\ Mg_{0.48})$	$(Si_{7.92}\ Al_{0.08})$	$O_{20}\ (OH)_4$	$Na_{0.48}\ Ca_{0.04}\ Mg_{0.02}$
octahedral cations	tetrahedral cations	structural O/OH	exchangeable cations

The cation exchange capacity is around 0.8 eq/kg bulk material. The natural exchangeable cations are sodium (~85%), calcium (~10%), magnesium (~4%) and small amounts of potassium (~0.3%). The specific surface area is around 550 m^2/g material and the grain density is around 2,750 kg/m^3.

The target density for LOT test parcel A2 at full water saturation was 2,000 kg/m^3. The actual values fall in the range 1,900–2,000 kg/m^3 (Karnland et al. 2009).

2.4 The near field environment

Initially, a limited amount of air will be left in a repository and in a bentonite test parcel after emplacement, which during the water saturation phase will be partly trapped by the low permeability rim of groundwater-saturated bentonite (King et al. 2001, 2010). After water saturation the chemical environment in the immediate vicinity of the copper surface is determined by the composition of the bentonite pore water. This is, in turn, determined by the interaction between the bentonite and the saline groundwater in the surrounding rock. The entrapped oxygen will be consumed through reactions with minerals in the rock and the bentonite, through copper corrosion, and also through microbial activity.

After the oxygen has been consumed, corrosion will be controlled by the supply of dissolved sulphide to the copper surface. However, this anoxic period is beyond the scope of the present study which concerns the oxic period.

Table 2-1. The actual groundwater composition from the Äspö Hard Rock Laboratory.

Ion	mM	mg/dm^3
Na^+	100	2,300
K^+	0.28	11
Ca^{2+}	47.3	1,896
Mg^{2+}	2.4	58
Cl^-	178	6,311
HCO_3^-	0.44	27
SO_4^{2-}	4.6	442
HS^-	0.005	0.15
pH 6.9±0.1	Eredox -308 mV (SHE)	

3 Experimental

LOT test parcel A2 was retrieved from the Äspö HRL in January 2006. After retrieval of the test parcel shown in Figure 1-2b, a bentonite test package containing the cylindrical copper electrodes was first furnished with a copper sheet on the outside (to be used as a counter electrode) and then placed in a plastic container, equipped with two reference electrodes, and sealed with a thick layer of paraffin to maintain an environment alike the one before retrieval. Later on the same year new copper and platinum electrodes were installed in the test package.

During 2006 electrochemical measurements were performed on the pre-exposed and additional new electrodes at the Royal Institute of Technology (KTH) in Stockholm (Rosborg and Pan 2008).

In January 2007 the bentonite test package was transported by car from KTH to the Slovenian National Building and Civil Engineering Institute (ZAG) in Ljubljana for installation of electric resistance (ER) sensors in the test package. The prime objective of the ER measurements was to facilitate the interpretation of the results from the real-time corrosion monitoring with electrochemical techniques that has been performed both before and after retrieval of the LOT test parcel. The results from the ER measurements are presented in this report together with back-up information from electrochemical measurements and post-test examination of the ER sensors and retrieved copper coupons. Results from the work have earlier been presented (Rosborg et al. 2011a, b), however, the present report is an all-inclusive account of the work performed.

All measurements reported below have been performed at room temperature.

3.1 Retrieval of test package

3.1.1 Performance

Figure 3-1 shows how LOT test parcel A2 was retrieved from the Äspö HRL, how the bentonite test package consisting of bentonite rings 35–37, which contained the pre-exposed copper electrodes, was cut off from the test parcel after removal of the surrounding rock, and how the bentonite test package was sealed with a thick layer of paraffin (on all sides). The top end of the central copper tube was the only part of the original test parcel sticking out of the paraffin layer, Figure 3-1f.

A copper sheet was placed on the outside of the bentonite test package next to the pre-exposed copper electrodes in bentonite ring 36, and the two standard reference electrodes (Appendix A) were installed in the bentonite test package just before covering the top of the test package with paraffin.

3.1.2 Effect on pre-exposed copper electrodes

It is obvious from the real-time corrosion monitoring results shown in Figure 3-2 that the pre-exposed copper electrodes were greatly disturbed during retrieval of the test parcel. The electrochemically *recorded* corrosion rate before retrieval was about 1.5 μm/year[5] and it increased significantly (see Figure 3-2a), and the corrosion potential changed considerably after retrieval (Figure 3-2b) (Rosborg and Pan 2008). During the retrieval procedure the copper electrodes experienced mechanical disturbance from the decreased bentonite swelling pressure, drilling and cutting operations, and a temperature excursion of about 10°C (Karnland et al. 2009).

[5] The value was calculated by using n=2 in Faraday´s law and with no correction for the measuring frequency used, see (Rosborg 2013). A better estimate of the corrosion rate yields a value below 0.8 μm/year (Rosborg et al. 2004).

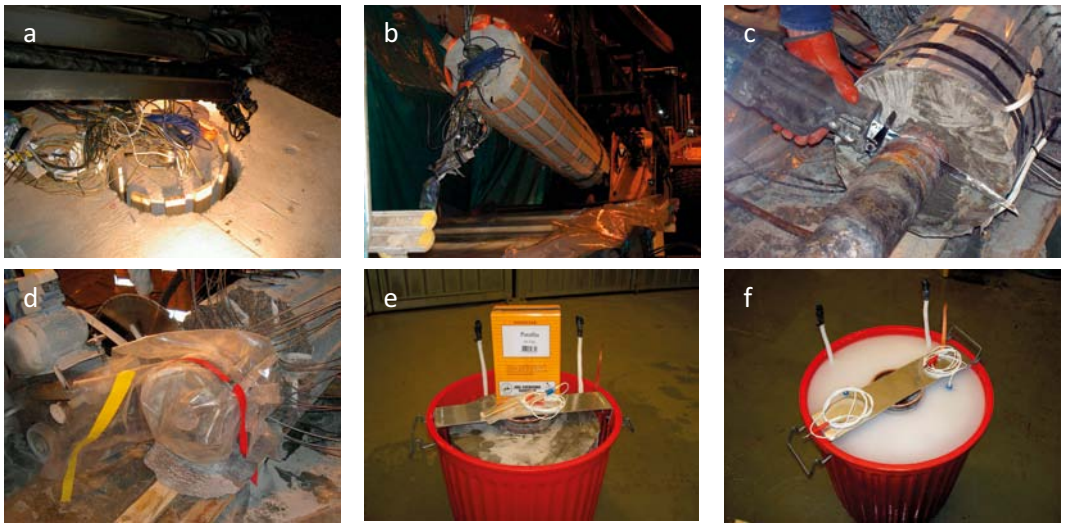

Figure 3-1. *Retrieval of the pre-exposed copper electrodes in January 2006. (a-b) Lift-up of LOT test parcel A2 with surrounding rock, (c-d) cutting off the bentonite test package after removal of surrounding rock, and (e-f) moulding the bentonite test package in paraffin.*

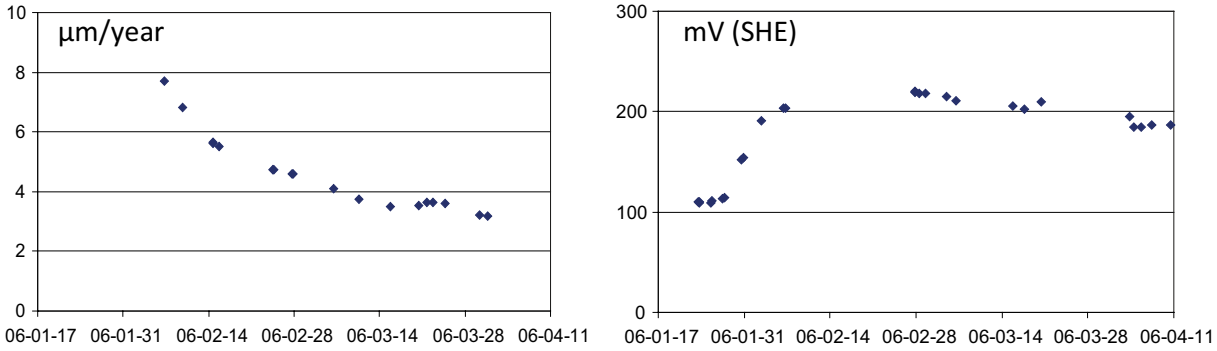

Figure 3-2. *(a) The electrochemically recorded corrosion rate in µm/year and (b) the corrosion potential in mV (SHE) of one of the pre-exposed copper electrodes after retrieval. (Time on the x-axis is given as yy-mm-dd.)*

3.1.3 Anticipated environmental conditions after retrieval

After retrieval the conditions for the pre-exposed copper electrodes in the bentonite test package were anticipated to be similar but of course not the very same as before, since the pressure on the bentonite test parcel in the rock has been relieved.

Concerning temperature, bentonite ring 36 was at 24°C in the Äspö HRL and after retrieval held at room temperatures. Thus it has almost always been exposed to about the same temperature. During the retrieval procedure it experienced a temperature excursion of about 10°C.

A thick paraffin layer covered the bentonite test package on all sides, but for the top of the central copper tube, which was exposed to the surrounding environment, Figure 3-1f. From start of exposure it was not clear how the inside would be influenced by the surrounding air. However, the paraffin layer has been penetrated a few times when new copper and platinum electrodes have been installed in the test package, and repetitively when the liquid junction to the reference electrodes was refurbished. Additionally, small quantities of aerated Äspö groundwater were added, see below.

The evolution of the corrosion potential of the copper samples in the test package should give some information about the environment and its stability with time, see also below, and similar corrosion potentials and *recorded* corrosion rates were established for the pre-exposed and new copper electrodes with time (compare Figures 3-3a and 3-3b).

The recorded exponential Tafel coefficients for the pre-exposed copper electrodes before and after retrieval of the bentonite test package indicate that the corrosion conditions are not identical after retrieval. Before retrieval the anodic and cathodic Tafel coefficients were about the same at 13 mV (Tafel slopes[6] about 30 mV per decade) (Rosborg et al. 2005). Long after retrieval the Tafel coefficients differ somewhat and are higher (typically about 25 and 28 mV respectively).

3.2 ER measurements

ER measurements to estimate the corrosion rate of a metal are based on the fact that a decrease in thickness of a metallic conductor causes an increase in electric resistance (ASTM G96 – 90(2008)). In practice the electric resistance of a corroding sensor element is compared to that of a corresponding corrosion protected reference sensor element. The reference element also compensates for resistivity changes due to temperature. The sensitivity of an ER sensor is defined by its thickness, but a lower thickness also means a shorter service life of the sensor. Thus, a trade-off exists between sensor sensitivity and sensor life. ER sensors generally do not distinguish between general and localized corrosion forms. A post-test examination is required to reveal the appearance of the corrosion damage and to verify the results.

To estimate the corrosion rate during the performance of a test, uniform corrosion is assumed and a nominal corroding surface area is used as a default value for calculations. An uneven corrosion attack on the sensor will influence the calculated rate. Corrosion on the sides of plane sensor leads can have a strong impact on the obtained result. Thus, there is an obvious need for a post-test examination of the sensor to find the actual distribution of corrosion damage and to evaluate its influence on the recorded corrosion rate.

Four ER sensors with the ZAG design made of pure copper, each with a thickness of 35 µm, were installed in the bentonite test package in January 2007. The fabrication and installation of the ER sensors are briefly described in section 3.2.1 together with the measurement procedure and a description of how the nominal thickness change with time has been calculated.

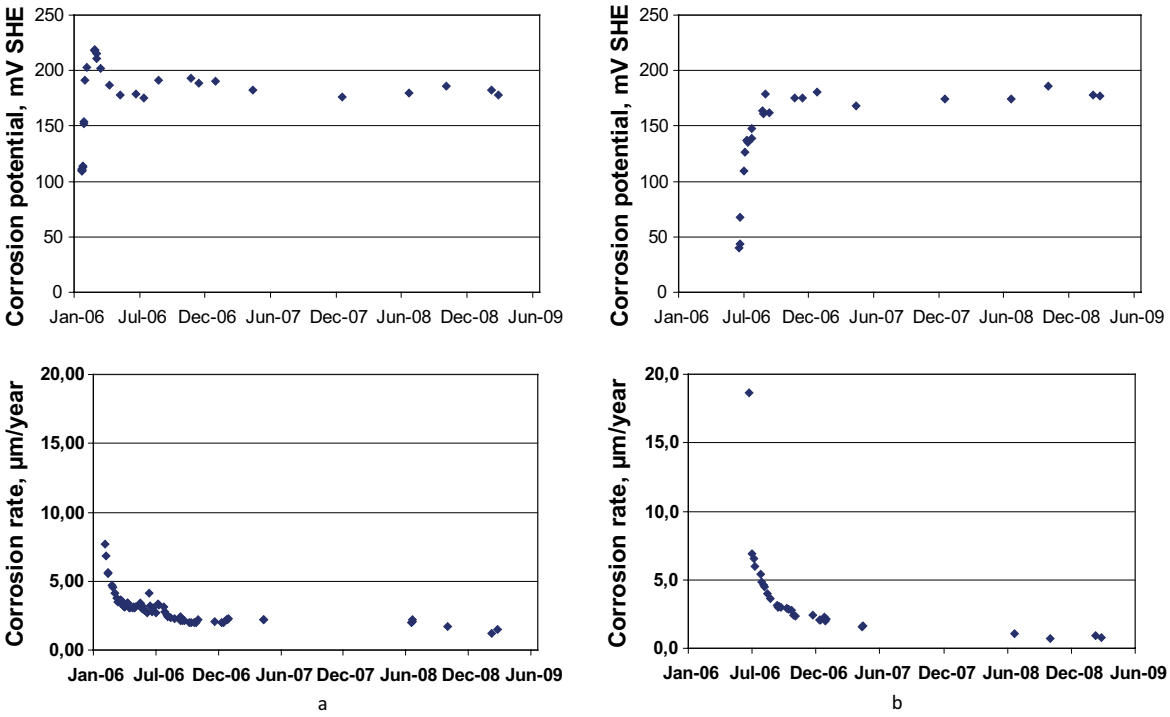

Figure 3-3. *The evolution of the corrosion potential and the electrochemically recorded corrosion rate for (a) the pre-exposed and (b) the new copper electrodes in the bentonite test package.*

[6] Tafel slopes ≈ 2.3×Tafel coefficients (Cottis and Turgoose 1999).

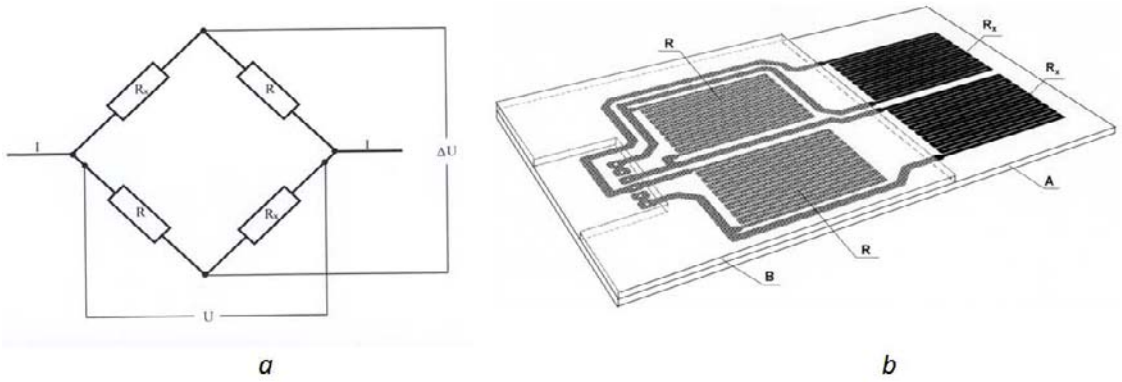

Figure 3-4. *(a) The Wheatstone bridge arrangement, and (b) the positions of the sensor (R_x) and reference (R) elements on and between glass-fibre resin plates (A and B) in the ZAG design.*

3.2.1 Fabrication of sensors

The ER sensors that were used to measure the corrosion rate of pure copper in the bentonite test package were designed and manufactured by ZAG in Ljubljana. In the ZAG design thin metal foils are first hot-glued on a glass-fibre resin plate. Sensor and reference elements are then manufactured by a photo-chemical process and etched similar to printed circuits for electronic equipment (Legat and Kuhar 2008). The corroding sensor and reference elements are positioned in a Wheatstone bridge arrangement, see Figure 3-4. Pictures of sensor elements and an ER sensor ready to be installed is shown in Figure 3-5. The reference sensor elements are protected by a glass- fibre epoxy resin plate as shown in Figures 3-4b and 3-5c. The soldering joints are protected by a chemical resistant elastic polymer as shown in Figure 3-5c.

In short, 35 µm thick copper foils[7] of electronic grade oxygen-free copper (Copper No. C10100; min 99.99% Cu) were first hot-glued on a glass-fibre resin plate with a thickness of 1.5 mm and then photo-chemically etched to obtain sensor elements of the form shown in Figure 3-5. The procedure used for gluing involves pressing the copper foil on to the resin-plate resulting in deformation of the copper foil next to the resin plate, as seen in Figure 3-5b. The width of the electric lead in the sensor element was about 0.7 mm.

The nominal surface area of one sensor element was about 3.5 cm^2 and two sensor elements form the corroding part of the ER sensor. (Thus, a default value of $2 \times 3.5 = 7.0$ cm^2 should be used to estimate the corrosion rate of the ER sensors from electrochemical measurements during exposure. However, since a sizeable part of the sensors has corroded away during the exposure, see below, the final surface areas could in principle be estimated from the post-test examination of the sensors in order to gain a better estimate of the final corrosion rate.)

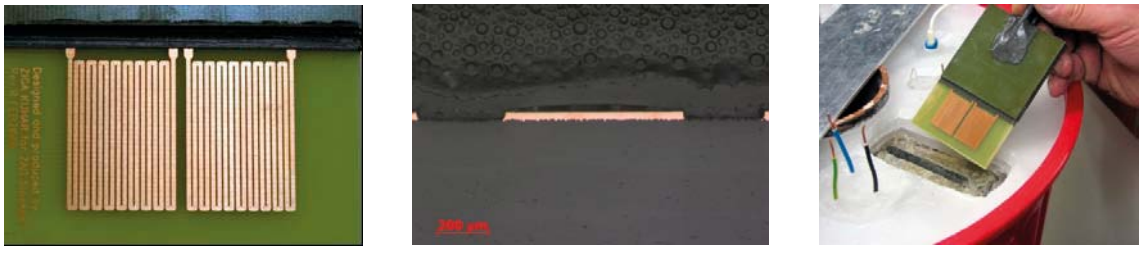

Figure 3-5. *Pictures of (a) two sensor elements, which represent two parts in the Wheatstone bridge arrangement (Figure 3-4), (b) a cross-section through the 35 µm thick and about 700 µm wide electric lead, and (c) an ER sensor ready for installation showing the corroding sensor elements seen on the resin plate and the reference elements (not seen) in between the glass-fibre resin plates to the upper right in the picture.*

[7] The final thickness of the foil was in fact obtained by electroplating.

3.2.2 Installation of sensors

The ER sensors were installed in pairs in the bentonite test package, with one sensor on each side of the glass-fibre resin plate. Figure 3-6 shows a series of pictures taken during the installation showing the positions of the ER sensors in the bentonite test package.

After removal of the paraffin layer a row of holes was drilled in the bentonite and formed into a slot. One side of the slot was made planar, and wetted with Äspö groundwater before one ER sensor was placed on it. Then, the open part of the slot on the other side of the sensor pair was back-filled with bentonite borings. During the back-filling the bentonite was repetitively wetted with Äspö groundwater. Thus, the installation procedure for the sensors on each side of the glass-fibre resin plate is not the same.

3.2.3 Performance of measurements

The ER measurements were started immediately after installation of the ER sensors on 2007-01-23 at 14:25 and were performed regularly since then with a break between 2010-03-05 and 2011-01-31. More than 400 series of readings were taken using first an older and later new equipment (338 series with the old equipment from start of measurements up to 2010-03-05[8], and 143 series with the new equipment from 2009-06-12 up to 2011-04-14[9] with an overlap of 79 series of readings; a few measurements were also performed after the bentonite test package had been cut in pieces, see below.) The new equipment had a better thermal stability and resolution of the voltmeter.

The input DC current was 50 mA and the output U and ΔU voltages are defined in Figure 3-4a. The frequency of measurements was twice a week or more during the periods of measurements. (To avoid accidental electric disturbances each reading with the old equipment was repeated until two consecutive readings gave the very same value. There was no need to repeat the readings with the new equipment.)

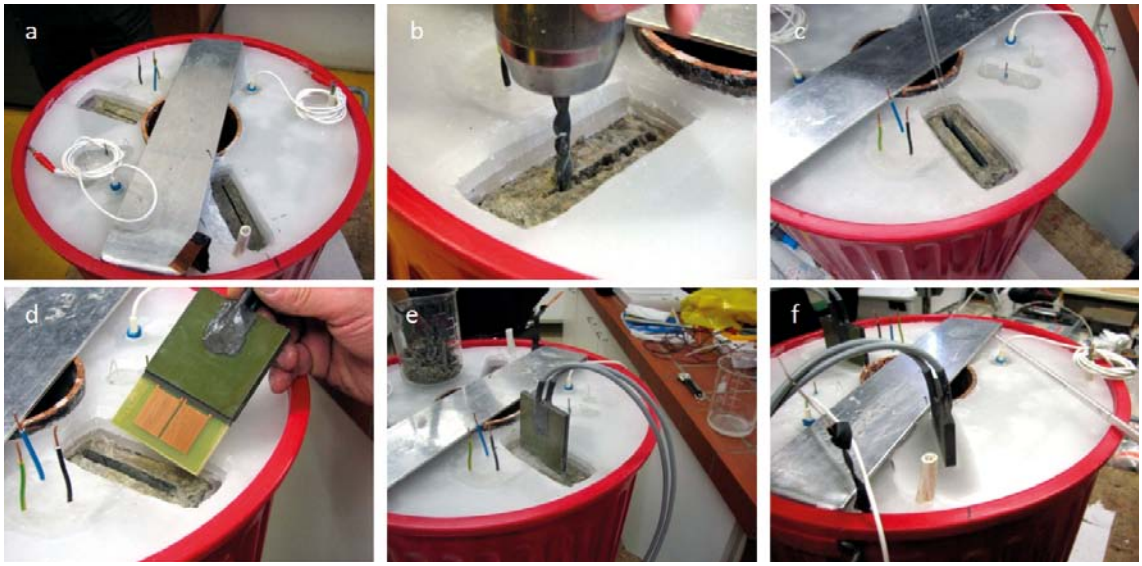

Figure 3-6. *Installation of the two ER sensor pairs in January 2007. (a) The paraffin layer removed at five and ten o´clock in the picture with positions for the sensor pairs marked, (b) drilling a row of holes in the bentonite, (c) a slot has been formed, (d) one sensor pair about to be placed in the slot, (e) ditto in place in the bentonite, and (f) both sensor pairs installed and the paraffin layer restored.*

[8] CRA 2000 Corrosion Analyzer, Institute "Jožef Stefan", Ljubljana, Slovenia.

[9] A PCS-100 Portable Current Source combined with a Fluke 289 True RMS Multimeter.

3.2.4 Nominal thickness change with time

The resistance of an electric lead is calculated by the formula

$$R = \rho \frac{l}{A}$$

where R=resistance, ρ=resistivity of the metal, l=length, and A= the cross-sectional area of the electric lead. A decrease of the latter with ΔA will cause an increase in the resistance corresponding to ΔR and ΔA can be written as

$$\Delta A = A \frac{\Delta R}{R + \Delta R}$$

When the corrosion on both corroding sensor elements is uniform and thus the same, the output voltages U and ΔU shown in Figure 3-4a can be calculated to be

$$U=(R_x+R)\frac{I}{2}$$

$$\Delta U=(R_x-R)\frac{I}{2}$$

Since $\Delta R = R_x - R$

$$\frac{\Delta U}{U} = \frac{\Delta R}{2R + \Delta R}$$

and substituting $\frac{\Delta U}{U}$ with u allows ΔR to be written as

$$\Delta R=\frac{2u}{1-u}R$$

The decrease of the cross-sectional area can now be written as

$$\Delta A = A \frac{\Delta R}{R + \Delta R} = A \frac{\frac{2u}{1-u}R}{R + \frac{2u}{1-u}R} = A \frac{2u}{1+u}$$

For the used sensor elements A = d · w, where d= thickness and w=the width of the electric lead. The original thickness (d_o) and width (w_o) of the electric leads were 35 µm and about 0.7 mm respectively. Ignoring the change in width of the leads during exposure, the decrease of the sensor thickness with time can thus be estimated by the formula

$$\Delta d = d_\circ \frac{2u}{1+u} = 35 \frac{2u}{1+u}$$

3.3 Electrochemical measurements

The corrosion potentials of all the copper samples in the bentonite test package were measured to gain information about the redox conditions in the bentonite/saline groundwater environment, its stability with time, and the stability of the corrosion potential for individual samples. The corrosion potentials of the ER sensors have regularly been measured since May 2007.

Electrochemical impedance spectroscopy (EIS) and real-time corrosion monitoring techniques have also been applied to estimate the corrosion rates of the ER sensors in the above environment. Electrochemical measurements have also been performed on the other copper samples in the bentonite test package, as reported elsewhere (Rosborg and Pan 2008, Rosborg et al. 2004).

3.3.1 Corrosion potential measurements

The corrosion potentials of the ER sensors (and of the other copper samples) in the bentonite test package have been measured against a saturated silver-silver chloride reference electrode. Since the bentonite eventually "consumes" the liquid junction between the bentonite and the reference

electrodes, the following replenishment procedure has been applied. The reference electrodes were removed and examined for the presence of solid crystals in their reference solution compartments. If needed solid potassium chloride crystals and additional reference solution were added. New liquid junction solution in the form of Äspö groundwater was then added, and the reference electrodes reinstalled in the bentonite test package and sealed with paraffin. The experimental procedure is described in more detail in Appendix A.

As a consequence of this procedure small quantities of Äspö groundwater were repetitively added to the bentonite/saline groundwater environment. No attempt was made to deaerate the groundwater before addition.

3.3.2 Electrochemical impedance spectroscopy

EIS measurements were regularly performed on the four ER sensors, Table 3-1. The first series of measurements was performed on 2007-05-14 and twelve series were performed with the latest on 2011-03-08. An introduction to EIS, and how to estimate corrosion rates from EIS data, can be found in Cottis and Turgoose (1999).

Gamry Reference 600™ potentiostats controlled by Gamry EIS 300 software were used for the three-electrode measurements. Strictly, each measurement was performed under potentiostatic control, with the working electrode potential locked to its open circuit value. A saturated calomel electrode was used and the external copper sheet (electrode area > 1 dm^2) served as the counter electrode. The amplitude of the applied sinusoidal voltage was 5 mV rms and seven data points per decade were recorded. A frequency range from 100 kHz down to 1 mHz was applied, but for the most recent test series measurements were started from 1 MHz (and a Faraday´s cage was used).

Different methods can be applied to estimate the polarization resistance, R_p, from impedance data, Appendix B.

The polarization resistance, Rp, of the ER sensors was estimated from the impedance data in two ways: (i) it was arbitrarily taken as the absolute impedance |Z| at 1 mHz (the lowest frequency applied for the majority of measurements) ignoring the electrolyte resistance[10], and (ii) it was estimated by fitting EIS data to equivalent circuits (Cottis and Turgoose 1999). Further information on the evaluation is given in Appendix B. The corrosion current density and the corrosion rate were then calculated by the same procedures.

Table 3-1. Performed EIS measurements with the same instrumental set-up. Gamry Reference 600™ potentiostats; cell configuration: ER sensor/saturated calomel electrode/external copper sheet as counter electrode.

Item	Date	ER1	ER2	ER3	ER4
0	*2007-01-23*		*Installation of ER sensors*		
1	2007-05-14	x	x	x	x
2	2007-10-30	x		x	x
3	2008-01-08	x		x	x
4	2008-04-22	x		x	x
5	2008-07-09	x		x	x
6	2008-10-16	x		x	x
7	2009-01-14	x		x	x
8	2009-04-14	x	x	x	x
9	2009-11-24	x	x	x	x
10	2010-02-05	x	x	x	x
11	2010-02-06	x	x	x	x
12	2011-03-08	x	x	x	x

[10] Since the electrolyte resistance is lower than 1% of the absolute impedance it has been ignored in the present calculations.

EIS measurements performed earlier on the pre-exposed and new copper electrodes in the bentonite test package are reported elsewhere (Rosborg and Pan 2008).

From the R_p-values, listed in Appendix B, the corrosion current density, i_{corr}, was calculated with the Stern-Geary equation (Stern and Geary 1957)

$$i_{corr} = \frac{B}{R_p}$$

using a B-value of 15 mV. The B-value was obtained from the SmartCET® corrosion monitoring performed on the ER sensors in October 2008, Appendix D.

The corrosion rate (expressed as a penetration rate) was then calculated using Faraday´s law (ASTM G102 – 89(2010))

$$CR = 3.27 \frac{i_{corr}}{d} \frac{W}{n}$$

where CR is the corrosion rate in µm/year, i_{corr} the corrosion current density in µA/cm^2, d the density in g/cm^3, W the atomic weight (dimensionless), and n the number of electrons required to oxidize an atom. For pure copper d=8.94 g/cm^3 and W= 63.54 and thus the corrosion rate in µm/year is

$$CR = 23.3 \frac{i_{corr}}{n}$$

or for a B-value of 15 mV

$$CR = \frac{349}{R_p \cdot n}$$

3.3.3 SmartCET® corrosion monitoring

The real-time corrosion monitoring on the pre-exposed copper electrodes before and after retrieval of the bentonite test package, and on the new copper electrodes, was performed with a SmartCET® corrosion monitoring system and a three-electrode cell configuration[11]. This involves polarization resistance and harmonic distortion analysis techniques used to derive information regarding the general corrosion rate (Scully 2000, Darowicki and Majewska 1999). A voltage perturbation with a frequency of 0.01 Hz and a 50 mV peak-to-peak amplitude is applied and the current response is measured and analyzed synchronously with the perturbing sine wave. The harmonic distortion analysis involves the measurement of the higher harmonic content at 0.02 and 0.03 Hz, which then allows the anodic and cathodic Tafel coefficients and the Stern-Geary coefficient to be estimated. The applicability and accuracy of the obtained data has been discussed (Rosborg et al. 2005).

SmartCET® corrosion monitoring has also once been applied on the ER sensors for a fairly short period. In October 2008 it was found that the corrosion potential of the ER sensors were close to the potential of the saturated silver-silver chloride reference electrode, see below. Thus, it was possible to establish three-electrode configurations with two ER sensors and the silver-silver chloride reference electrode, the latter being substitute for one of the ER sensors (for instance sensor ER1– reference electrode – sensor ER3) and with the three electrodes far apart. Since the ER sensors were installed in pairs in the test package it was not possible to use three ER sensors only; this had resulted in a too poor cell geometry (Thompson and Payer 1998).

Objections can be raised to the use of this method under the above circumstances: the surface area is quite small considering the very low corrosion rates, and the cell geometry is unfavourable.

3.3.4 The electrochemical frequency modulation technique

Like SmartCET® corrosion monitoring the “Electrochemical Frequency Modulation” (EFM) technique also gives values of the corrosion current and the corrosion rate without knowing the Tafel slopes

[11] SmartCET® Technology – User Guide v06 04 03, InterCorr International, Houston, TX.

and the Stern-Geary coefficient beforehand (Bosch and Bogaerts 1996, Bosch et al. 2001). It is a small signal AC technique in which two sine waves (of different frequencies) are applied to the electrochemical cell simultaneously. The current response contains not only the input frequencies, but also frequency components which are the sum, difference, and multiples of the two input frequencies. More information about the method is found in Appendix C.

So-called single-shot EFM measurements have been performed on the ER sensors. A Gamry Reference 600™ potentiostat and Gamry EFM140™ software were used for the measurements. Due to lack of prior experience with the method, a series of measurements using different amplitudes and base frequencies was first tried.

Certain objections have been raised to this method (Kuş and Mansfeld 2006).

3.4 Post-test examination

A post-test examination of the ER sensors has been performed to gain information about the corrosion products, the type and localization of the corrosion attack on the sensors, and to measure the final dimensions of the ER sensors to obtain average corrosion rates.

3.4.1 Cutting of bentonite test package

On 2011-04-12 the bentonite test package was cut into sections at Clay Technology in Lund. The bentonite sections containing each set of electrodes and sensors were placed in tri-laminate[12] bags that were air-evacuated; one bentonite section contained the sensor pair ER1/ER2 and another the sensor pair ER3/ER4. Figure 3-7 shows the sensor pair ER1/ER2 still in place in the remaining part of the bentonite package during the cutting process; the sensor pair ER3/ER4 had already been removed. The tri-laminate bags with the ER sensors, Figure 3-8, were then brought to ZAG in Ljubljana by air on 2011-04-13 for the post-test examination.

Figure 3-7. *The sensor pair ER1/ER2 just before removal from the bentonite test package.*

[12] plastic/aluminium/plastic.

Figure 3-8. *Evacuated tri-laminate bags with the two sensor pairs (and another bentonite piece).*

3.4.2 Removal of bentonite

The post-test examination was started with the sensor pair ER1/ER2 and the analytical procedure developed step by step before analysing the sensor pair ER3/ER4. Before starting the removal of the remaining bentonite from the sensor pair an ER measurement was performed. The sensor pair ER1/ER2 was then removed from its bentonite section and finally split apart to allow the examination of each sensor. The initial work on sensor ER1 was focused on identifying the corrosion products on the sensor, and the initial work on the failed sensor ER2 was focused on finding the failure on the sensor elements and examine the localization of the corrosion attack. A series of photographs were taken during and immediately after removal of the bentonite from the sensors.

A photo of the bentonite piece with the sensor pair immediately after opening its tri-laminate bag is shown in Figure 3-9.

The last ER measurements before transport of the bentonite test package to Clay Technology for cutting were performed on 2011-04-10. After opening the tri-laminate bag to start the post-test examination at ZAG, a single ER measurement was then performed on sensor ER1 on 2011-04-14 with the sensor pair ER1/ER2 still in place in the bentonite piece. (The accompanying sensor ER2 had earlier failed.) Finally, a single measurement was also performed on 2011-10-29, when sensors ER1 and ER2 had been split apart. The results from the two measurements are included in Figure 4-12a.

Figure 3-9. *Photo of sensor pair ER1/ER2 on top of its tri-laminate bag.*

The procedure used to remove the bentonite from the sensor pair is shown in Figure 3-10. Two cuts were first made along the sides of the glass-fibre resin plate sticking out of the bentonite piece (cuts 1 and 2), and when the bottom ends of the resin plate were seen on both sides a third cut was made along the bottom part of the resin plate (cut 3). Figure 3-11 shows that the bentonite was easily removed using a knife, and had a soap-like consistency .

In the next step the two remaining bentonite sections on the sensor pair were removed by bending, Figure 3-12, with the exposed surfaces shown in Figures 3-13 and 3-14. It is obvious from the figures that bentonite still remained on the sensor elements and some of the corrosion products are attached to the removed bentonite sections.

Finally the sensor pair was split apart as shown in Figure 3-15. Sensor ER1 with its adjacent bentonite section was then immediately handed over for analysis of the corrosion products on the sensor elements and on the adjacent bentonite. Sensor ER2, which failed quite early during exposure, was forwarded to microscopy.

These procedures were then used on sensor pair ER3/ER4.

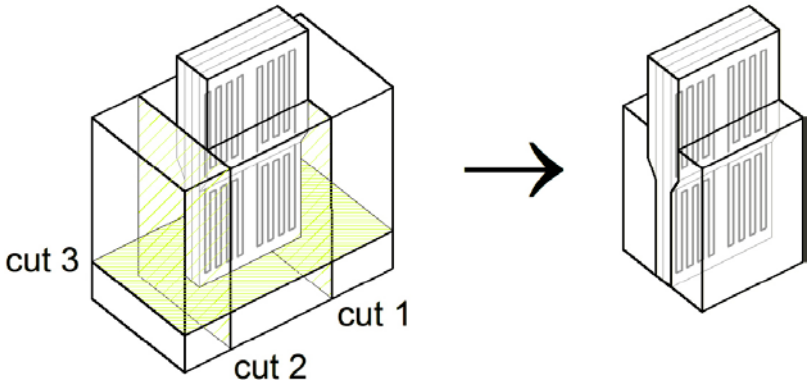

Figure 3-10. *Procedure used for removing surrounding bentonite from the sensor pairs.*

Figure 3-11. *Removing bentonite by knife to make one side of the resin plate visible (cut 1).*

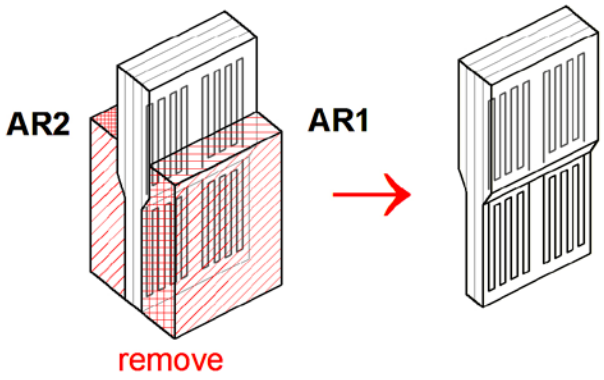

Figure 3-12. *Removing the remaining bentonite sections (AR1 and AR2) from the sensors.*

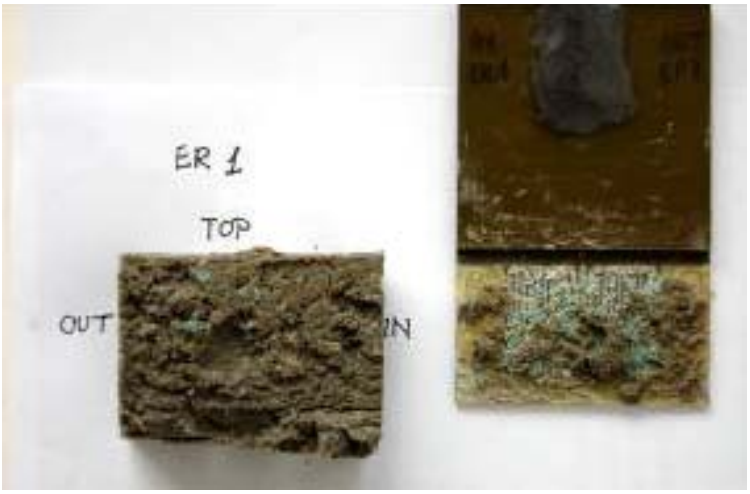

Figure 3-13. *Appearance of sensor ER1 after removal of the last bentonite section.*

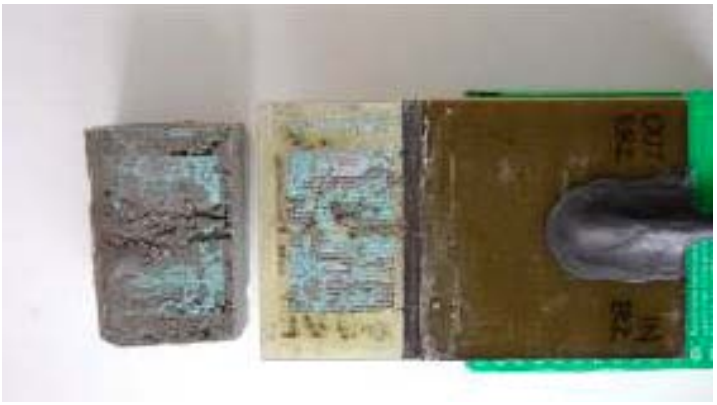

Figure 3-14. *Appearance of sensor ER2 after removal of the last bentonite section.*

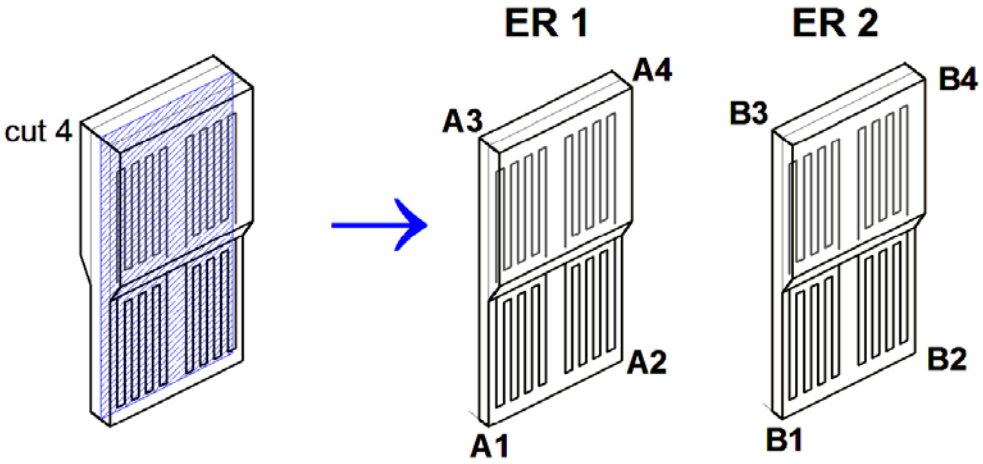

Figure 3-15. *Separation of sensors ER1 and ER2 with identification of sensor elements, designated A1–A4 and B1–B4.*

3.4.3 Identification of the corrosion products

Information about the corrosion products is needed to better interpret results from the EIS measurements and to more accurately express the corrosion rates as penetration rates.

The x-ray diffraction (XRD) measurements[13] on corrosion products scraped from sensor ER1 were performed on 2011-04-16. One sample contained mainly brownish corrosion products and another contained blue-green corrosion products. The background noise from bentonite (reflections from constituents in the bentonite) was extensive for the latter sample.

Raman spectroscopy[14] was performed on sensor ER1 on 2011-04-15 using a 514 nm laser excitation line, a long working distance 100x objective and a 600 grooves/mm grating, which gave a spectral resolution of 1.99 cm^{-1}/pixel. The power at the sample surface was set between 0.14 and 14 mW. A multi-channel air-cooled CCD[15] detector was used with integration times between 20 and 35 s. The obtained spectra are presented after baseline correction.

3.4.4 Type and localization of corrosion

The appearance of the corrosion damage on the ER sensors was first documented in a series of photographs taken immediately after removal of the bentonite.

Examination of the sensor surfaces was also done by light microscopy, and by scanning and dual-beam electron microscopy[16].

It was considered important to examine the ER sensors for any localization of corrosion damage: first to find out how localization of corrosion on a sensor element affected the recorded corrosion rates, and secondly to explain the different behaviours of the ER sensors. An extensive effort was made to measure cross-sections of exposed and protected sensor elements.

[13] Using a D4 ENDEAVOR XRD system and DIFFRAC. EVA software from Bruker AXS GmbH, Karlsruhe, Germany.

[14] Using a LabRAM HR800 Raman spectrometer from Horiba Jobin Yvon coupled to an Olympus BXFM optical microscope.

[15] Charge-coupled device.

[16] A Nova 600 NanoLab DualBeam™-SEM/FIB microscope from FEI Company, 5350 NE Dawson Creek Drive, Hillsboro, OR 97124-5793, USA.

3.4.5 Final dimensions of ER sensors

A first estimate of the average corrosion rate of an ER sensor can be obtained from the ER readings by merely dividing the final nominal thickness change Δd (section 3.2.4) by the exposure time. This was anticipated to overestimate the actual corrosion rate, yielding a conservative value. However, the average corrosion rate can also be obtained by comparing cross-sections of corroded and non-corroded (reference) sensor elements on the same ER sensor. It is assumed that the final and original cross-sections of the electric lead in a corroded sensor element are proportional to the final and original weights of the electric leads per unit length. Since meaningful weight measurements could not be applied, this "geometric method" is a substitute, and should supply a better estimate of the actual average corrosion rate.

For this reason the areas of the cross-sections of the electric leads in corroded and protected (reference) sensor elements from the very same ER sensor have been measured. Each ER sensor contains four sensor elements, Figure 3-4, and a plane through each sensor element contains 18 cross-sections of the electric lead. (However, due to sampling for other purposes a few sections of the lead parts were not available for the measurements.)

The areas of the cross-sections were measured in the following way: The metallographic samples containing the sensor elements were cut, grinded and polished with a 1 µm polycrystalline diamond suspension. The cross-sections were then viewed on a Carl Zeiss AXIO Imager M2z metallographic microscope equipped with AXIO VISION 9/2009 software. The areas of the cross-sections were measured with image analysis using the Multiphase software. (Sensor ER2 had been ultrasonically cleaned in 10% sulphuric acid solution before measurements, which however should not invalidate the result (Rendahl 1998).)

From the average area of cross-sections from protected electric leads, A_i, and corroded electric leads, A_f, the average corrosion rate based on the area change, CR-ΔA, was estimated as follows (where the inverse number ratio denotes the exposure period in years):

$$\text{CR-}\Delta\text{A}\ (in\ \mu m/year) = 35\ \frac{\text{Ai} - \text{Af}}{\text{Ai}}\ \frac{365}{1539}$$

3.5 Supporting information from copper coupons

The copper coupons (dimensions 60×15×1.5 mm) that were exposed in bentonite rings 22 and 30 of LOT test parcel A2 (at temperatures of 75 and 30°C respectively) for six years, see section 2, supply background information of relevance for the interpretation of the results obtained from the ER measurements.

3.5.1 Corrosion products

After six years exposure in the bentonite/saline groundwater environment at the Äspö HRL the copper coupons had accumulated a brownish corrosion product layer with blue-green corrosion products covering most of the surface (Karnland et al. 2009). Figure 3-16a shows the appearance of a copper coupon immediately after breaking apart the bentonite section containing the coupon. Corrosion products can also be seen adhering to the bentonite surface facing the copper coupon.

X-ray diffraction measurements confirmed that the main constituent of the brownish corrosion product layer is cuprite, Cu_2O, and that the blue-green corrosion products are paratacamite, $Cu_2(OH)_3Cl$.

3.5.2 Localization of the corrosion damage

A tendency to localization of the corrosion attack has been observed; the general corrosion is unevenly distributed on the copper surface as visualized in Figure 3-16b. No signs of active pits have been found. Similar observations have earlier been reported (Litke et al. 1992).

3.5.3 Average corrosion rate

The average corrosion rate of pure copper calculated from weight measurements of the copper coupons before and after exposure was found to be less than 0.5 µm/year. This corrosion rate is lower than the recorded values from the SmartCET® corrosion monitoring of the copper electrodes exposed in bentonite ring 36 both before and after retrieval (Figure 3-2). Possible reasons for the overestimation of the corrosion rate by the electrochemical methods were discussed previously (Rosborg et al. 2005). One evident reason is that the corrosion rate is merely overestimated by not using a sufficiently low measuring frequency (0.01 Hz) to obtain the true polarization resistance.

a

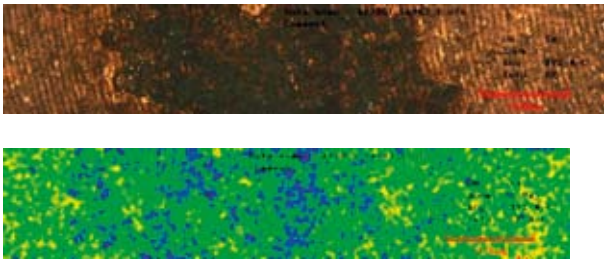

b

(Top) Photograph of a corroded surface, and (bottom) a visualization of the localization of the corrosion damage obtained by image analysis, where the colour blue depicts the deepest penetration sites.

Figure 3-16. *(a) Appearance of a copper coupon after six years exposure in the bentonite/saline groundwater environment at Äspö, and (b) localization of the general corrosion attack on one of the copper coupons.*

4 Results

Corrosion potentials recorded on the ER sensors are shown below and compared to the corrosion potentials measured on the pre-exposed and new copper electrodes in the bentonite test package. The reason for this is to assess the redox conditions in the exposure environment, to determine whether stable conditions have been achieved and to relate the ER sensors behaviour to that of the copper electrodes made from solid canister material. The corrosion products and appearance of the corrosion damage on the sensors are also shown and discussed. Then the recorded corrosion rates from the ER and electrochemical measurements are presented. Finally, based on information obtained from the post-test examination average and final corrosion rates are given.

4.1 Corrosion potentials

The evolution of the corrosion potential with time for the ER sensors is shown in Figure 4-1 together with the recorded electrode potential for a platinum electrode in the test package. Selected primary data from these measurements are presented in Appendix A.

In Table 4-1 the corrosion potentials for the ER sensors are compared to the corrosion potentials measured on the cylindrical copper electrodes (from the three-electrode set-ups in the bentonite test package). The corrosion potentials for the ER sensors have, with time, achieved higher values than those measured on pre-exposed and new copper electrodes manufactured from actual copper canister material. In all cases the positive values indicate the presence of oxic conditions in the test package. The platinum values point to stable redox conditions during the exposure of the ER sensors.

4.2 Corrosion products

On removing the bentonite from the sensor pair ER1/ER2, it was obvious from the colours of the corrosion products on the sensors that both Cu(I) and Cu(II) corrosion products had been formed during the exposure, Figure 4-2. The XRD measurements verified the presence of cuprite, Cu_2O, and paratacamite, $Cu_2(OH)_3Cl$, as shown for a sample analysis in Figure 4-3. This finding is consistent with analyses on copper coupons in the LOT test parcel A2 (Karnland et al. 2009). As observed on the coupons the blue-green corrosion products were loosely attached to the copper surface on the ER sensors.

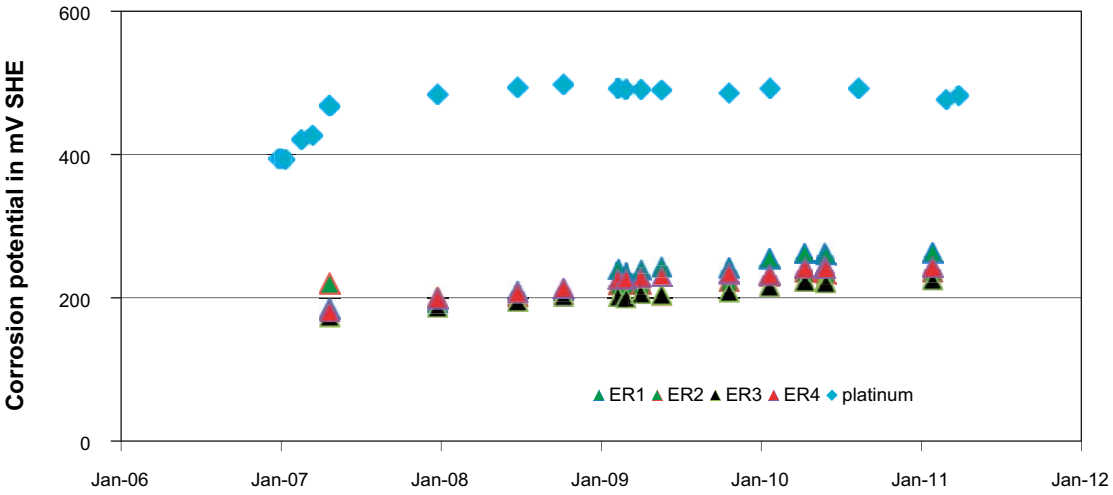

Figure 4-1. *Evolution of the corrosion potential with time for the ER sensors.*

Table 4-1. Corrosion potentials for copper samples in the bentonite test package (in mV (SHE)). (The measured ranges comprise values from three electrodes.)

Sample	May-07	Jan-08	Oct-08	Apr-09	Nov-09	Apr-10	Oct-10	Mar-11
ER1	**182**	**193**	**210**	**239**	**243**	**262**	**261**	**261**
ER2	**217**	**201**	**209**	**219**	**225**	**236**	**238**	**239**
ER3	**171**	**187**	**202**	**206**	**210**	**223**	**223**	**222**
ER4	**180**	**199**	**213**	**228**	**236**	**241**	**243**	**242**
Pre-exposed	182–196	176–188	186–194	179–190	180–188	184–206	180–204	178–198
New Cu	140–164	150–174	171–194	165–183	168–176	162–175	157–187	158–181

Figure 4-2. *The appearance of sensor ER1 after removal of corrosion products from part of the left sensor element (the brownish area).*

Raman spectroscopy on corrosion products still in place on sensor ER2 confirmed these findings, as exemplified by the spectrum shown in Figure 4-4. The band positioned at 508 cm^{-1}, the broad band at 897–971 cm^{-1}, and the bands at 3,358 and 3,437 cm^{-1} indicate the presence of paratacamite. (The high intensity of the Raman spectrum in the measured region is due to fluorescence from bentonite.)

4.3 Corrosion appearance

The appearance of sensor ER2 after removal of bentonite and also after cleaning in 10% sulphuric acid solution is shown in Figure 4-5. While the copper coupons from LOT test parcel A2 had blue-green corrosion products distributed periodically on top of a brownish corrosion product layer, Figure 3-16, the blue-green corrosion products on the ER sensors are much more abundant. The ER sensors in the bentonite test package obtained higher corrosion potentials, well above 200 mV (SHE), compared to the anticipated corrosion potentials of the copper coupons in LOT test parcel A2 (considering data in Table 4-1). The latter are not known but should be far lower and decreasing. Thus, the ER sensors have definitely been exposed longer at high corrosion potentials, which could explain the different corrosion appearance.

The post-test examination of the ER sensors revealed uneven corrosion on the exposed sensor elements varying from a slight attack to full penetration of the 35 µm thick electric lead, Table 4-2. Examples of remaining cross-sections from sensor ER2 are shown in Figure 4-6. An uneven distribution of general corrosion on copper exposed to bentonite clay has been observed previously (Litke et al. 1992, Karnland et al. 2000). The variation of the corrosion on sensors ER3 and ER4 is shown in Figure 4-7, and Figure 4-8 shows an almost complete penetration of the electric lead. Appendix E contains the quantitative information on the final dimensions of the ER sensors.

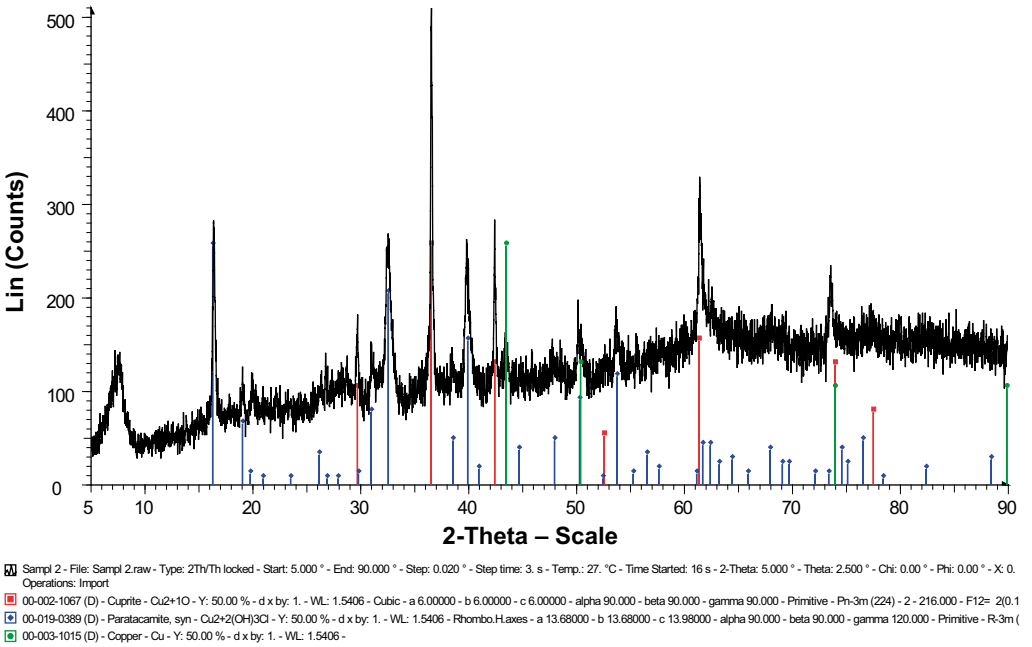

Figure 4-3. *XRD spectrum from corrosion products together with line spectra from cuprite (red), paratacamite (blue) and copper (green).*

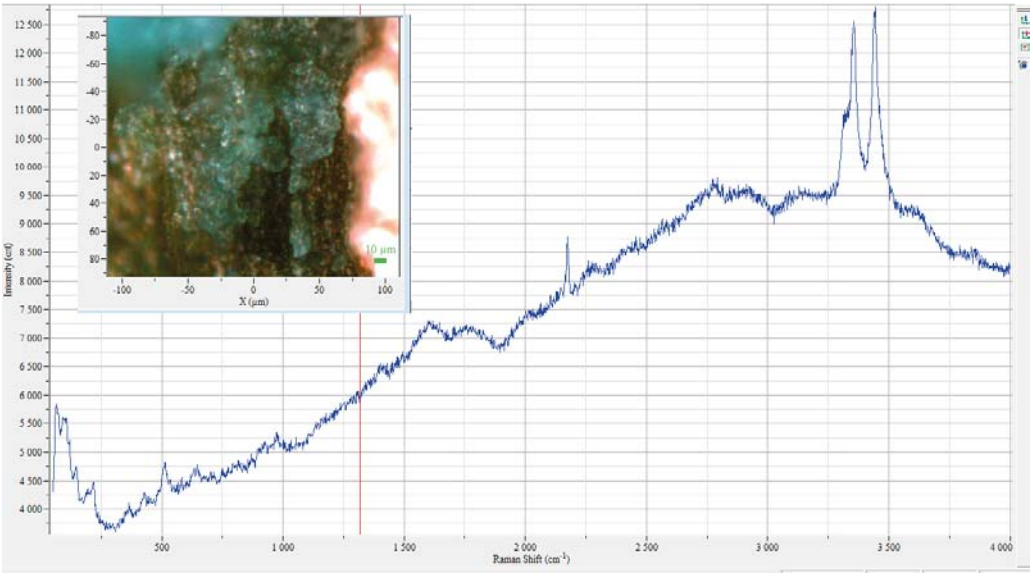

Figure 4-4. *A representative Raman spectrum recorded on the blue-green corrosion products on sensor ER2 seen in the inset.*

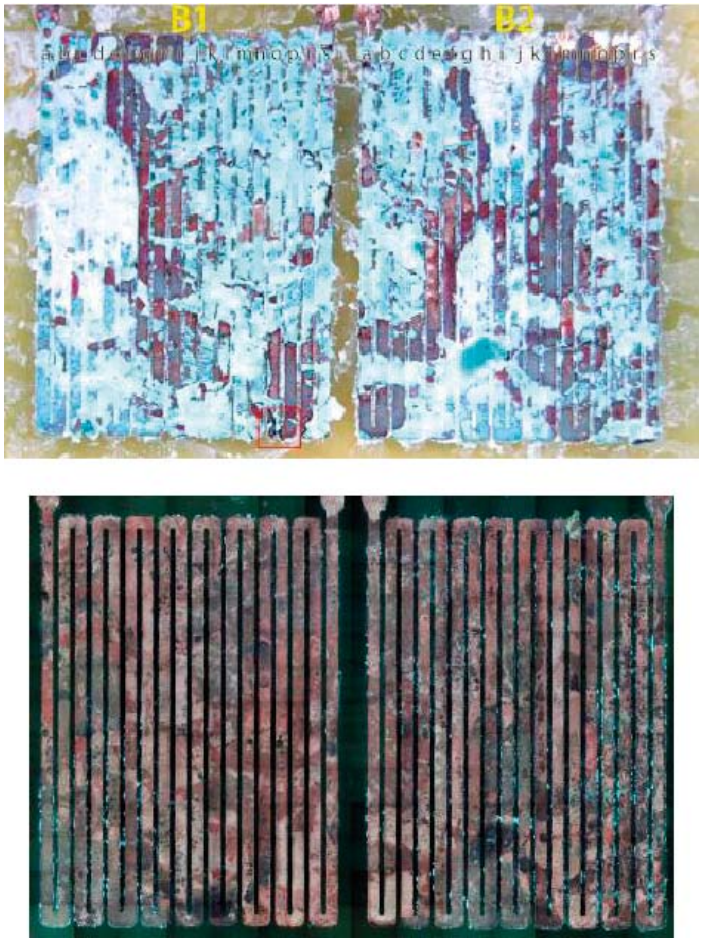

Figure 4-5. *Appearance of sensor ER2 (top) after removal of the adjacent bentonite piece and (bottom) after the first ultrasonic cleaning in 10% sulphuric acid solution.*

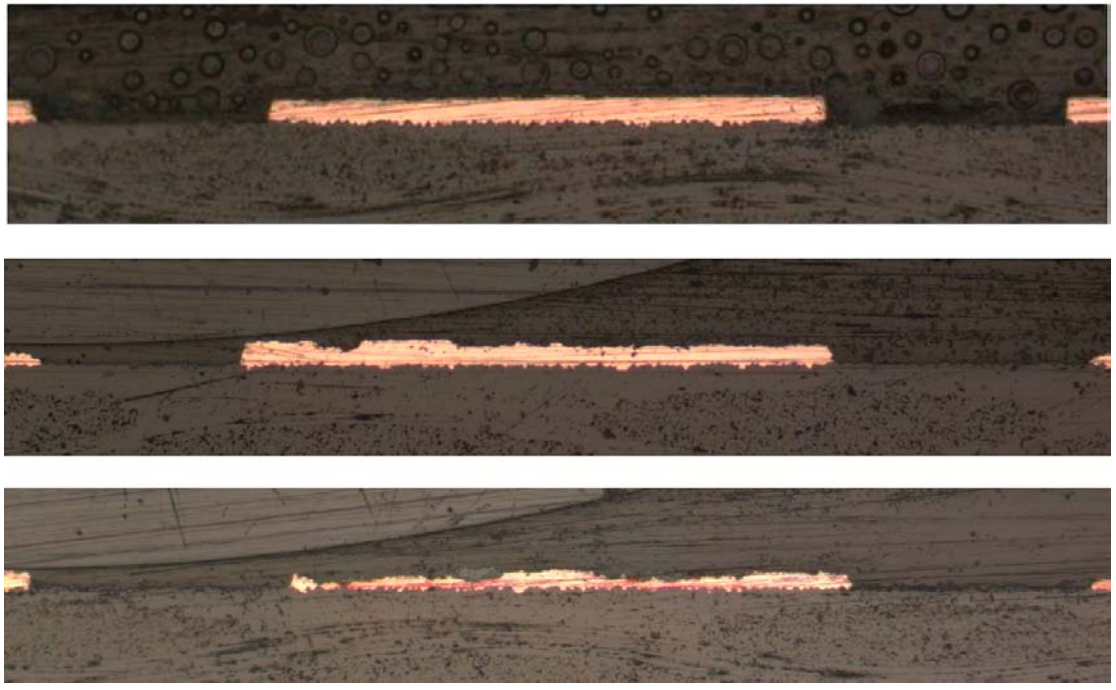

Figure 4-6. *Examples of cross-sections of a corroded electric lead in sensor ER2. (A cross-section of the electric lead in a protected sensor element is shown in Figure 3-5.)*

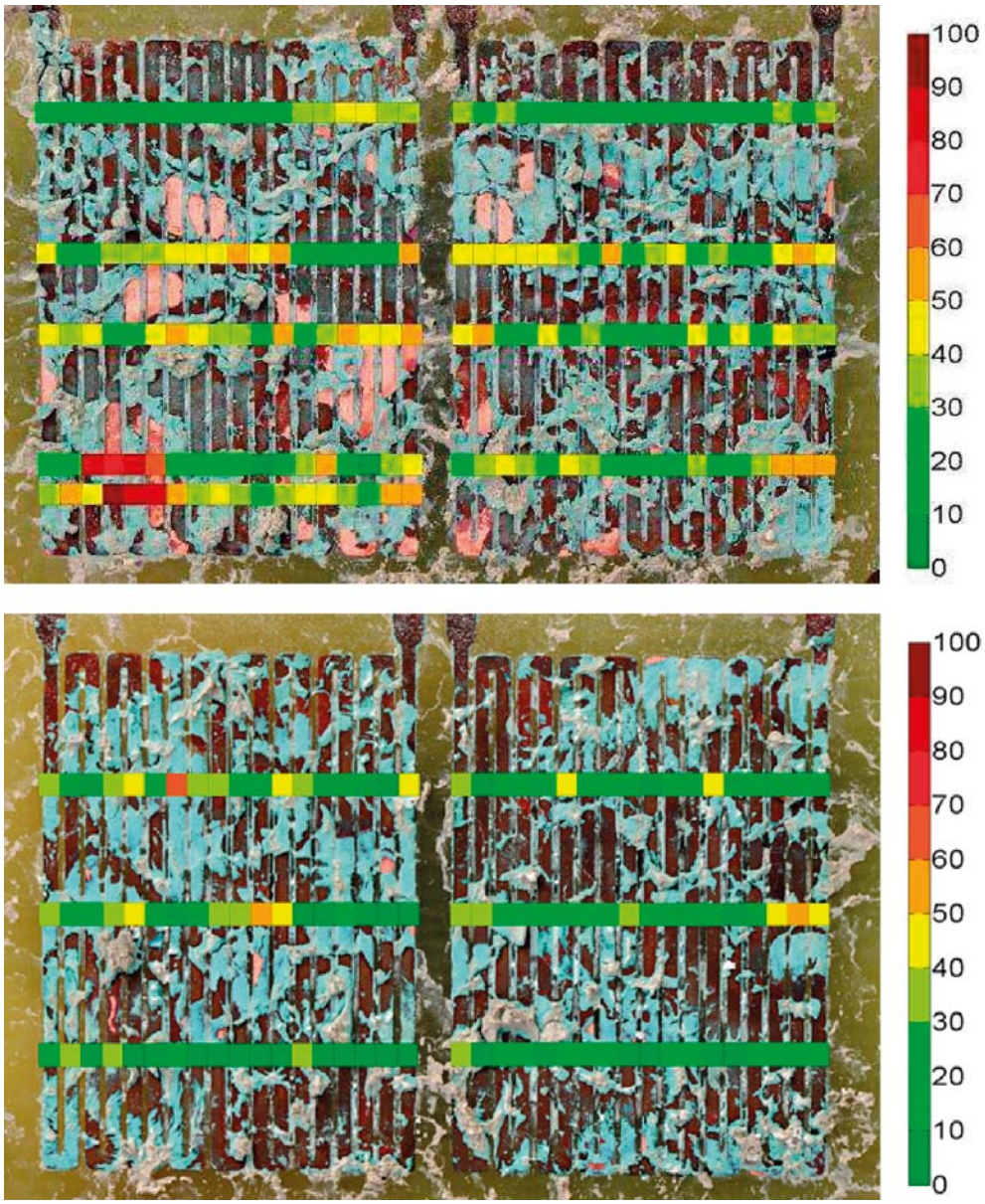

Figure 4-7. *Optical images illustrating the localization of corrosion on sensors ER3 (top) and ER4 (bottom). The scale to the right and the different colours used define the corrosion depth, from no attack (dark green at 0) to full penetration (brownish red at 100). The bands made up of parts with different colours visualize information obtained by microscopy described in section 3.4.5.*

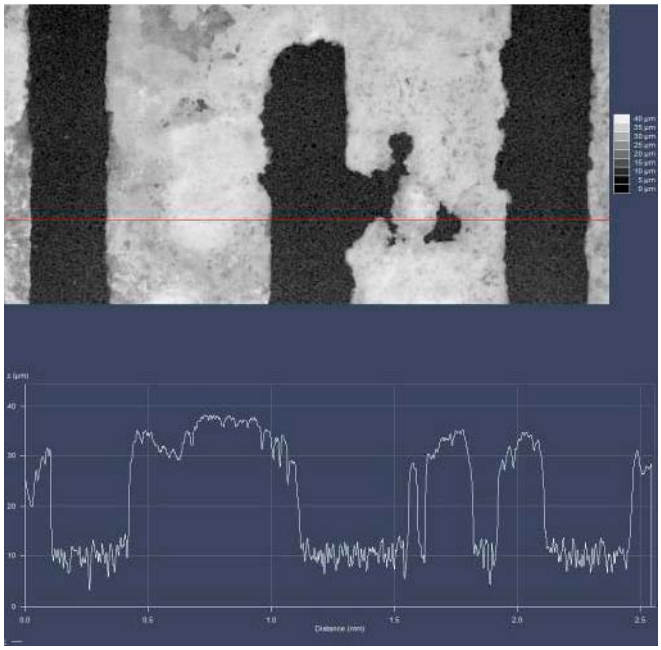

Figure 4-8. *Example of a local penetration of the electric lead in sensor ER2. The bottom picture shows the profile of the sensor lead in the top picture along the red line.*

Figures 4-9 and 4-10 show a magnified image of the surface of sensor ER1 after exposure, and Figure 4-11 shows a micro cross-section though the corrosion product film on the surface, which varies considerably in thickness.

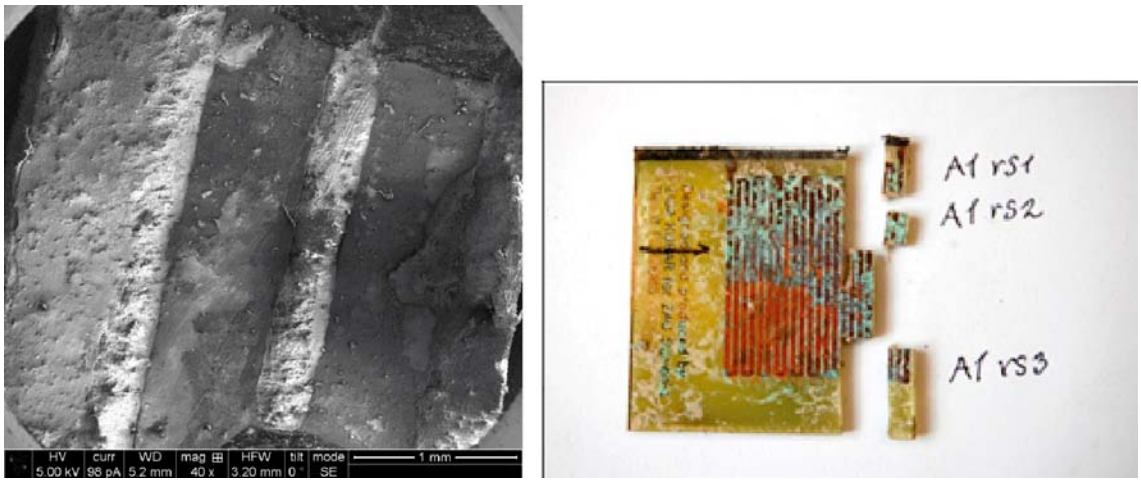

Figure 4-9. *Low magnification image of the surface of sensor ER1 after exposure (sample A1 rs3; SEM).*

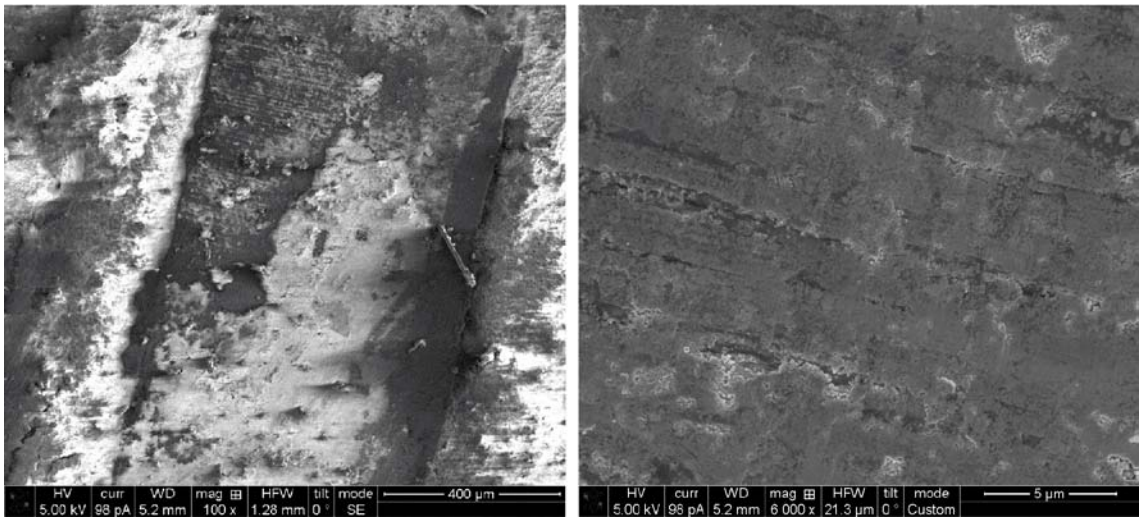

Figure 4-10. *High magnification image of the surface of sensor ER1 (sample A1 rs3; SEM).*

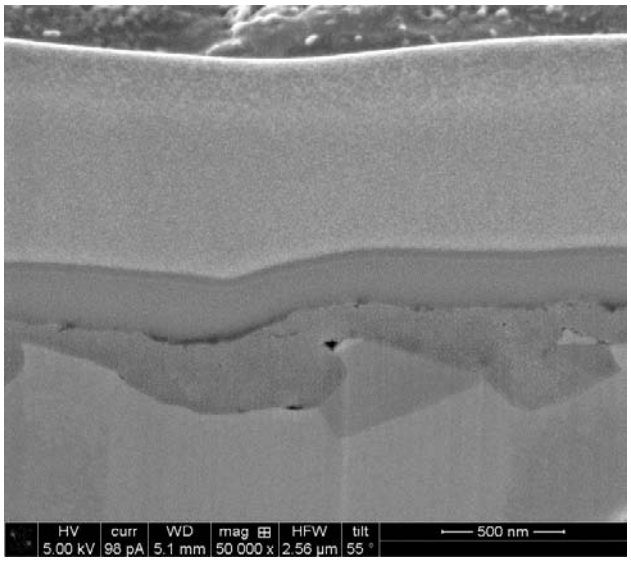

Figure 4-11. *Micro cross-section from sensor ER1 (sample A1 rs3; SEM/FIB microscopy). (The irregular grey area in between the two platinum deposits on top, one thick pale-grey and one thinner grey, and the copper metal below constitutes the corrosion product layer.) (magnification 50,000x)*

4.4 Corrosion rates from ER data

4.4.1 Performance of sensors

While sensors ER1 and ER4 survived the four years (1,539 days) of exposure, sensors ER2 and ER3 failed after about four months and three years respectively. Figure 4-12a shows that a sizeable amount of the sensor thickness has corroded away. In the following section some general comments on the performance of the sensors are first given, followed by comments on the specific performance of each sensor.

Initial corrosion rates – A wide scatter in initial corrosion rates was observed, Figure 4-12b, most probably a consequence of the installation procedure described in section 3.2.2. Beyond the initial period Figure 4-12 shows sensors ER1 and ER4 behaved similarly during the period of exposure. The higher initial corrosion rate of sensor ER1 resulted in an almost 4 µm extra metal loss compared to sensor ER4, Figure 4-13a, which gave an average corrosion rate of 2.0 compared to 1.6 µm/year during the four years exposure, as discussed below.

Corrosion potentials – The corrosion potentials of the sensors, from the start of measurements in May 2007 up to the end of the exposure period fall in the range 171–262 mV (SHE). (See Appendix A for detailed information.)

Influence of EIS measurements – EIS measurements were performed on several occasions during the exposure of the ER sensors, Table 3-1. (The times for the EIS measurements have been marked with vertical lines in Figure 4-12b.) No obvious influence of the EIS measurements on the performance of the ER sensors was found.

Sensor ER1 – was installed in a pair together with sensor ER2 as described in section 3.2.2. Its corrosion potential, first measured on 2007-05-08, was 185 mV (SHE) and its final corrosion potential was 261 mV (SHE). The sensor survived the full test period despite almost half of its thickness being corroded away, Figure 4-12a. The ER readings showed a gradually decreasing corrosion rate from > 21 µm/year down to a final *recorded* corrosion rate of 0.7 µm/year. From the EIS measurements its final corrosion rate was estimated to be 0.3 µm/year, see below.

Post-test examination of the sensor revealed corrosion to be unevenly distributed. The final cross-sections for the corroded sensor elements, Appendix E, fall in the range 0.0043–0.0213 mm^2 with an average of 0.0164±0.0029 mm^2. Figure 4-6 shows examples of cross-sections from a corroded sensor element (belonging to sensor ER2). By comparing cross-sections on corroded and protected sensor elements an average corrosion rate over the four years of exposure was estimated to be 2.0 µm/year, section 4.6. Using the same method the average corrosion rate at the locations for the cross-sections varies from less than 0.1 to 6.6 µm/year.

The information obtained from sensor ER1 has been assembled in Table 4-2 together with comparable information from the other ER sensors.

Sensor ER2 – failed after 140 days of exposure. Its corrosion potential was at start of exposure somewhat higher compared to the other sensors; while the latter have shown gradually increasing corrosion potentials during the entire exposure, sensor ER2 showed the highest value of all sensors in May 2007 (217 mV (SHE)) and a decreasing corrosion potential during 2007 which later again increased, see Figure 4-1 and for details also Appendix A.

Highly localized corrosion caused full penetration of the electric lead in one of the exposed sensor elements. Although this sensor experienced a local corrosion rate amounting to a material loss of 35 µm in four months, equivalent to a corrosion rate of 91 µm/year, the average corrosion rates of sensors ER1 and ER2 are not that different, Table 4-2. While failure of the sensor element made it impossible to follow the corrosion rate by ER measurements, it was still possible to follow it by electrochemical methods. From EIS measurements the final corrosion rate of ER2, after four years exposure, was estimated to 1.1 µm/year.

The mode of failure – was thus complete penetration of the electric lead in one of the exposed sensor elements due to localization of the general corrosion attack.

The cause of failure – is not known, but is most likely to be found in the adjacent bentonite. Accessory minerals in the bentonite may have caused localization of corrosion. Alternatively, the installation of the sensors, section 3.2.2, may have left groundwater and air-filled pockets at some locations next to the sensor that stimulated corrosion at these locations. (When the sensor was broken free from its surrounding bentonite, section 3.4.2, bentonite fragments were left on the sensor elements as shown in Figure 3-13. The failure was difficult to locate and the adjacent bentonite lost during removal from the sensor elements making a careful examination of the sensor surface impossible.)

Sensor ER3 – was installed in a pair with sensor ER4. The failure of this sensor occurred after a little more than three years exposure (observed after 1,135 days). The sensor showed an initially gradually decreasing corrosion rate down to a *recorded* value of about 7 µm/year, where it stayed until it finally failed, Fig. 4-12a. The mode and cause of failure are considered to be the same as for sensor ER2. From EIS measurements its final corrosion rate after four years exposure was estimated to be 0.5 µm/year.

Sensor ER4 – performed well over the entire exposure period and showed the lowest metal loss. ER measurements revealed a gradually decreasing *recorded* corrosion rate from > 16 µm/year to a final value of 0.8 µm/year, Fig. 4-13b. From EIS measurements its final corrosion rate has been estimated to 0.5 µm/year. Although it was anticipated that corrosion should be quite even, post-test examination of the sensor revealed that it was not.

Table 4-2 contains and compares information about the ER sensors.

4.4.2 Recorded corrosion rates

The *recorded* corrosion rates for the ER sensors are based on the assumption that corrosion is uniform. However, post-test examinations revealed that it was not, Figures 4-6 and 4-7; the depth of general corrosion varies considerably over the exposed sensor elements. (See also Appendix E for final dimensions of the ER sensors after exposure.) Thus, the *recorded* corrosion rates from the ER measurements are higher than the actual ones, as a decrease of the cross-section of the electric lead locally should result in an overestimation of the thickness change. A detailed evaluation of how much uneven corrosion affects the recorded values of the average thickness change with time is beyond the scope of the present report, and will be treated separately (Kranjc 2012). In the present report the *recorded* corrosion rates from the ER measurements are presented together with *recorded* values from the EIS measurements and *estimated* corrosion rates based on the final dimensions of the ER sensors determined by microscopy.

Figure 4-12a shows the nominal thickness changes with time for the four ER sensors. In the calculations the change of the original width of the electric leads (nominally 0.7 mm) is ignored, section 3.2.4. The recorded data for sensors ER1 and ER4 are expanded in Figure 4-13a. (ER readings from both the old and the new equipment are seen in the figure.)

Figure 4-12b shows the evolution of the *recorded* corrosion rates with time. At the start of exposure the corrosion rate was higher than 15 µm/year for all sensors. The spread in the initial corrosion rates is most likely a result of the differences in the installation procedure, described in sections 3.2.2 and 4.4.1. With time the corrosion rates for the two surviving sensors have slowly decreased to low but still measurable values, < 0.8 µm/year. Even after more than four years exposure the corrosion rates continued to decrease, Figure 4-13c.

Taking the small sensor thickness (comparable to surface roughness on manufactured components) in consideration, it is believed that the *recorded* corrosion rate for sensors ER1 and ER4 best reflects the true corrosion rate of pure copper in the bentonite test environment. (The recorded ER data for the failed sensors are deceptive and originate from malfunction of the sensors due to profound localization of the corrosion attack in these; on the same grounds the *recorded* corrosion rates from the two survivors are most probably overestimated.) When considering the data, it is wise to remember that the original thickness of the ER sensors of 35 µm is less than the surface roughness on a machined copper canister.

Table 4-2. Summary of rates and corrosion potentials for the ER sensors after four years exposure. (Corrosion rates, CR, in *µm/year* and corrosion potentials in *mV (SHE)*; pte=post-test examination and Local CR=the average CR at one cross-section.)

Sensor	Recorded values during exposure					Estimated values after pte				
	Initial CR	Corr pot		Final CR		Final areas of cross-sections		Average CR	Local CR	
	ER	Maj-07	Apr-11	ER	EIS	Range	Average		min	max
ER1	> 21	185	261	0.7	0.3	0.0043-0.0213	0.0164±0.0029	2.0	< 0.1	6.6
ER2	> 18	220	249		1.1	0.0000-0.0219	0.0144±0.0059	2.9	< 0.1	91
ER3	> 31	173	233		0.5	0.0000-0.0247	0.0169±0.0042	2.7	< 0.1	11.3
ER4	> 16	181	250	0.8	0.5	0.0090-0.0246	0.0182±0.0033	1.6	< 0.1	5.0

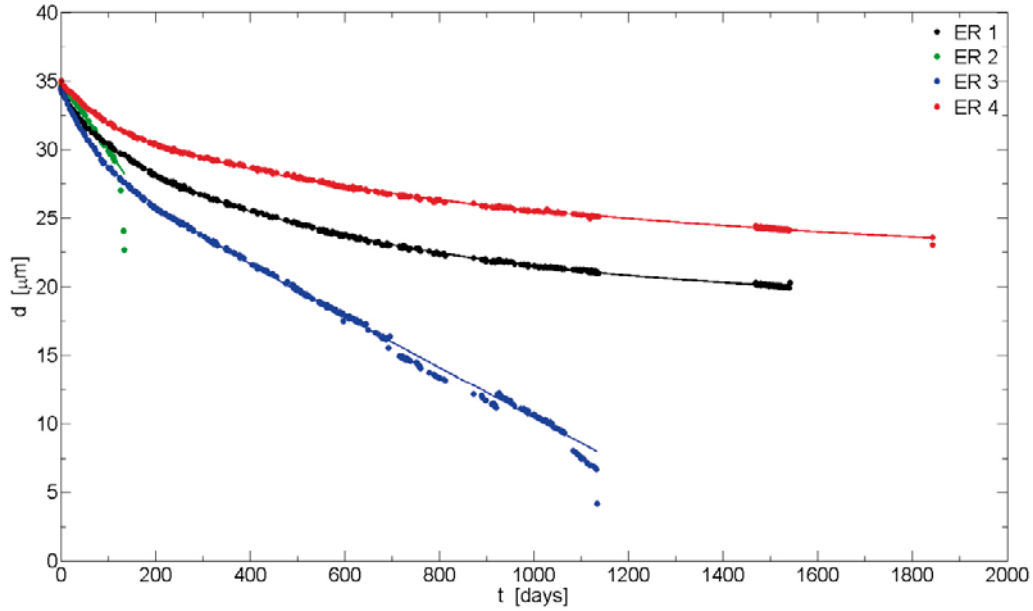

Figure 4-12a. *The recorded thickness change with time on the ER sensors.*

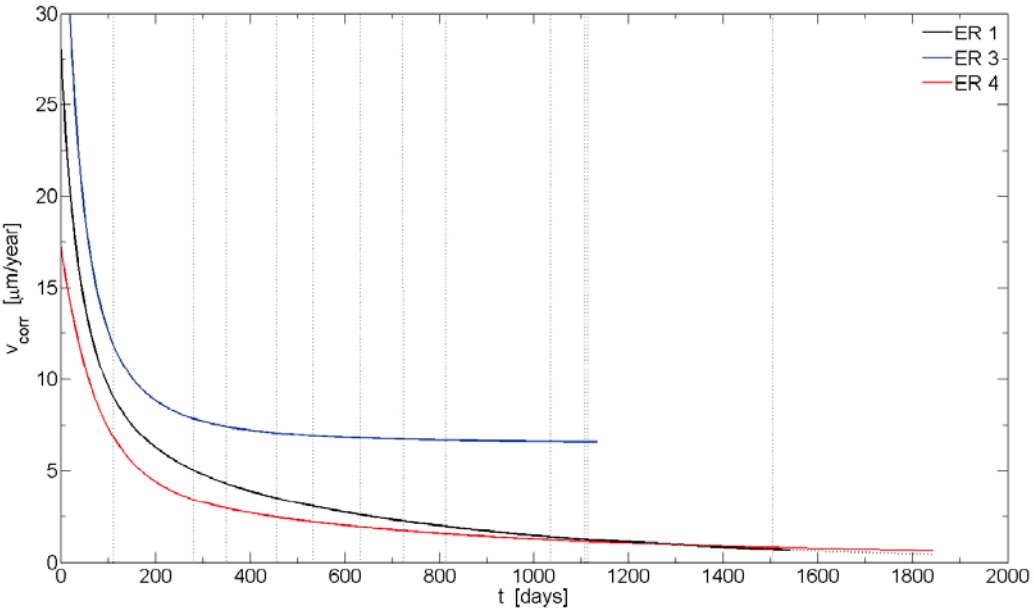

Figure 4-12b. *The estimated corrosion rate versus time for the ER sensors. (The vertical lines show when the EIS measurements were performed.)*

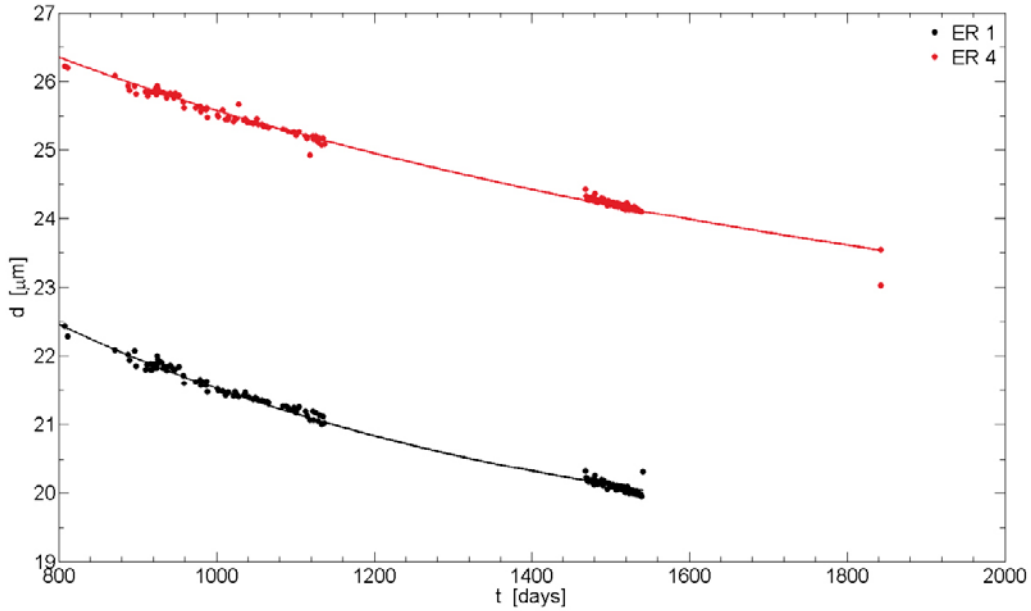

Figure 4-13a. *The nominal thickness change with time for sensors ER1 and ER4.*

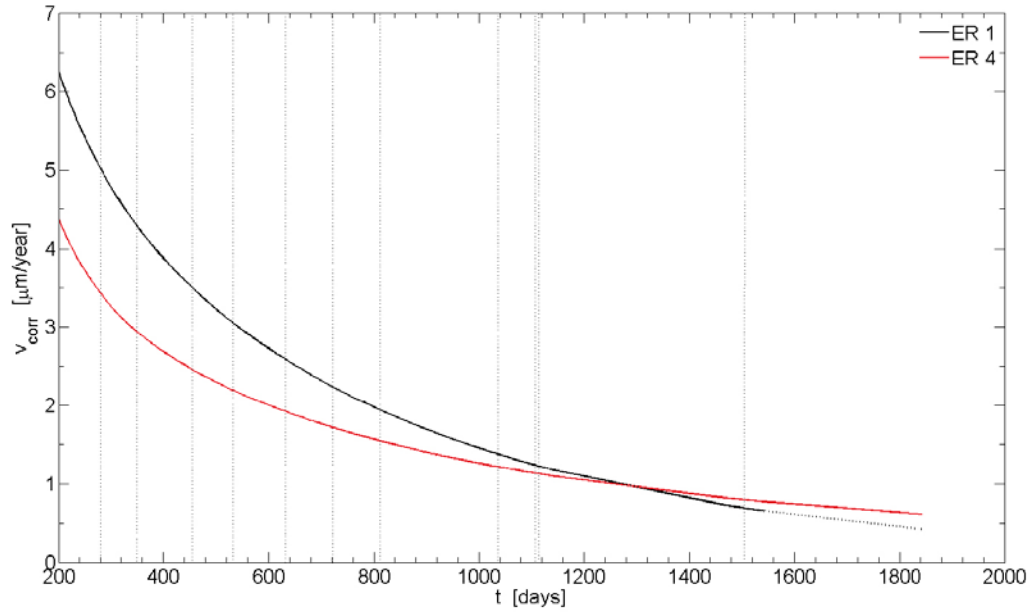

Figure 4-13b. *The estimated corrosion rate versus time for sensors ER1 and ER4.*

4.5 Corrosion rates from electrochemical data

The electrochemical measurements provide a corrosion current which can be converted to a corrosion rate by means of Faraday's law (ASTM G102 – 89(2010)). It is assumed that the current distribution is uniform and that the yield is 100% (i.e., that the total current results in corrosion).

Knowledge of the corrosion mechanism is needed to be able to use a proper equivalent weight when applying Faraday's law to convert the corrosion current to a penetration rate. The number of electrons required to oxidize a copper atom to a copper ion in the actual environment is either one (n=1) or two (n=2). Since both univalent and divalent corrosion products were formed, a compromise between these values has to be made. In this work the *recorded* corrosion rates during exposure have been given as a range using either n=1 or n=2 in Faraday's Law. (Estimates of the final corrosion rates from the EIS measurements based on a weighed n-value are given in section 4.6.)

4.5.1 From EIS measurements

The primary data from the EIS measurements on the ER sensors is treated in Appendix B. An example of recorded data is shown in Figure 4-14. The procedures used to first estimate the polarization resistance and then calculate the corrosion rate are described in section 3.3.2 and the appendix. The estimated corrosion rates from the EIS measurements are assembled in Table 4-3. The *recorded* corrosion rates were obtained by fitting the primary data to an equivalent circuit with three time constants.

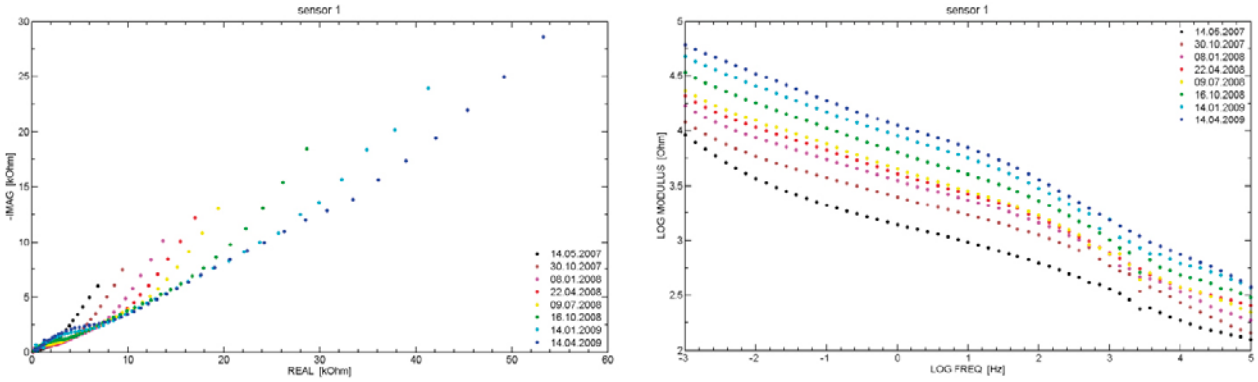

Figure 4-14. *The evolution of the Nyquist (to the left) and the modulus of the Bode (to the right) plots for sensor ER1 as a function of time.*

Table 4-3. Estimated corrosion rates for the ER sensors from EIS measurements. (The lowest value in the given ranges correspond to n=2 in Faraday's Law and the highest to n=1.)

Date	Days of exposure	Recorded corrosion rates in µm/year			
		ER1	ER2	ER3	ER4
2007-01-23		*Installation of ER sensors*			
2007-05-14	**111**	7.8-16			4.5-9.1
2007-10-30	**280**	3.5-7.0			2.7-5.4
2008-01-08	**350**	2.3-4.5			1.6-3.2
2008-04-22	**455**	1.5-2.9			1.5-3.1
2008-07-09	**533**	1.3-2.5			1.5-2.9
2008-10-16	**632**	0.6-1.3			1.1-2.1
2009-01-14	**722**	0.4-0.9			0.8-1.6
2009-04-14	**812**	0.4-0.8			0.7-1.3
2009-11-24	**1,036**	0.3-0.6			0.5-0.9
2010-02-05	**1,109**	0.3-0.6			0.5-1.1
2010-02-06	**1,110**	0.3-0.6			0.6-1.1
2011-03-08	**1,505**	0.2-0.4	0.7-1.4	0.3-0.6	0.3-0.7

4.5.2 From SmartCET® measurements

The recorded corrosion rates for the ER sensors from the SmartCET® measurements made in October 2008 are summarized in Table 4-4a. The primary data are found in Appendix D.

As a comparison, data recorded on a pre-exposed copper electrode just before retrieval and in October 2008 and on a new copper electrode (installed on 2006-06-20) also in October 2008 are shown in Table 4-4b.

Table 4-4a. Corrosion rates recorded on the ER sensors from SmartCET® measurements[17] made in October 2008.

Sensor	Recorded corrosion rates in µm/year	
	n=1	n=2
ER1	2.7	1.4
ER2	6.5	3.3
ER3	3.4	1.7
ER4	2.7	1.4

Table 4-4b. Corrosion rates recorded on pre-exposed and new electrodes from SmartCET® measurements.

Electrode set-up	Recorded corrosion rates in µm/year	
	n=1	n=2
Pre-exposed just before retrieval	3.0	1.5
Pre-exposed in October 2008	3.4	1.7
New in October 2008	1.6	0.8

4.5.3 From EFM measurements

Estimated corrosion rates from a test series of single-shot EFM measurements performed in April 2009 are shown in Table 4-5. The primary data are found in Appendix C.

Table 4-5. Corrosion rates recorded on the ER sensors in April 2009 using single-shot EFM measurements.

Sensor	Recorded corrosion rates in µm/year	
	n=1	n=2
ER1	2.6	1.2
ER2	7.7	3.8
ER3	4.1	2.1
ER4	3.1	1.5

4.6 Average and final corrosion rates

An estimate of the average corrosion rate can be obtained for sensors ER1 and ER4 by dividing the final recorded thickness change from the ER measurements by the exposure time. In this way the average corrosion rates for sensors ER1 and ER4 were estimated to be 3.4 and 2.6 µm/year respectively. However, a better estimate of the average corrosion rate was obtained by comparing cross-sections measured on corroded and protected electric leads. Table 4-6 presents the average corrosion rates estimated by the two methods described in section 3.4.5. (In the table Δd is the final recorded thickness change, CR-Δd the average corrosion rate based on this change, A_i the average cross-section of the protected electric leads in the sensor, A_f the average cross-section of the corroded leads in the sensor, and CR-ΔA the average corrosion rate based on the area change.)

[17] No correction for measurement frequency.

Estimates of the final corrosion rates of the ER sensors after four years of exposure are assembled in Table 4-7. Here the final corrosion rates from the ER measurements have been taken from Figure 4-13b, and the EIS measurements from Table 4-3 and altered as follows. Since quantitative information on the relative amounts of uni- and divalent corrosion products is lacking, it has been arbitrarily assumed after inspection of pictures of the ER sensors taken during the post-test examination that about equal amounts of each were formed. Thus, an average of the ranges of values have been taken from Table 4-3.

(Surface area corrections have not been made based on the following rationale: Before exposure the surface area of one sensor element was estimated to be 3.50 cm^2, where the top surface of the electric lead accounts for 18 × 0.0688 cm × 2.54 cm ≈ 3.146 cm^2, and the side surfaces for 0.32 cm^2, and the area of "connections" 0.038 cm^2. During exposure it is mainly the sides of the electric lead that decreased in nominal size. However, this will be counter-balanced by the roughening of all the surfaces. Thus, the overall area change should be fairly small, and has been ignored.)

Table 4-6. Estimates of the average corrosion rate for the ER sensors over the four years of exposure in the bentonite test package.

Sensor	Δd *µm*	CR-Δd *µm/year*	Average A_i *mm^2*	Average A_f *mm^2*	CR-ΔA *µm/year*
ER1	14.5	3.4	0.0215	0.0164	1.97
ER2	Not available		0.0221	0.0144	2.89
ER3	Not available		0.0250	0.0169	2.69
ER4	11.0	2.6	0.0226	0.0182	1.62

Table 4-7. Estimates of the final corrosion rates for the ER sensors after four years exposure. (The "From geometry" values originate from comparisons of cross-sections measured on corroded and protected electric leads.)

Sensor	Average corrosion rates in µm/year		Final corrosion rates in µm/year	
	From ER	From geometry	From ER	From EIS
ER1	3.4	2.0	0.7	0.3
ER2	–	2.9	–	1.1
ER3	–	2.7	–	0.5
ER4	2.6	1.6	0.8	0.5

5 Discussion

5.1 Corrosion behaviour of copper

The corrosion behaviour of copper in the bentonite test package is governed by the redox condition and composition of the bentonite pore water in contact with the copper surface (King et al. 2010). These properties have been determined by the interaction between the bentonite and the saline groundwater over six years of exposure in the Äspö HRL (Table 2-1). During retrieval of LOT test parcel A2 the corrosion conditions for the pre-exposed copper electrodes were disturbed, sections 3.1.2 and 3.1.3, and long after retrieval the conditions for the pre-exposed copper electrodes in the bentonite test package are anticipated to be similar to but not necessarily identical to those in the Äspö HRL, since the pressure on the bentonite in the rock has been relieved. Also, the recorded corrosion potentials, Figure 4-1, show it is reasonable to accept that conditions in the ER tests were oxic despite the presence of the thick paraffin layer. This can be attributed to air exposure on extraction from the bentonite, and the regular addition of air when refurbishing the reference electrodes, Appendix A.

The dominant corrosion stimulating species in the bentonite/saline groundwater environment are considered to be chloride ions and oxygen. The corrosion behaviour of copper in chloride media has been extensively reviewed (King et al. 2001, 2010, Kear et al. 2004). Most of the available data, however, refers to short test durations and few long-term exposure studies in repository environments have been performed.

The corrosion products on the ER sensors were found to be cuprite and paratacamite, in agreement with observations on copper coupons in LOT test parcel A2, section 3.5.1. The appearance of the corrosion damage on the ER sensors was also similar to that observed on the copper coupons in terms of both corrosion products and the localization of the corrosion. However, copper(II) corrosion products were more abundant on the ER sensors and the degree of localization more evident. While a copper coupon with an average corrosion loss of less than 3 µm after six years of exposure had a 17 µm deep penetration, one of the 35 µm thick ER sensors was completely penetrated in only four months. The reason for this is not obvious, but is most likely a result of the installation procedure.

Models for the time-dependent uniform corrosion of a copper canister in a deep geological repository exist (King et al. 2008).

5.2 Comparison with electrochemical data

On the condition that corrosion was uniformly distributed and that the resolution of the technique was good enough, it was first hoped that the ER measurements would be able to show whether the actual corrosion rate of pure copper in the bentonite/saline groundwater environment became lower than electrochemically recorded rates within one year. However, this turned out not to be the case as shown in Table 5-1a, which presents data from the first years of exposure. In the accompanying Table 5-1b the results from the ER and EIS measurements performed in 2010 and 2011 are compared and show that the corrosion rates obtained from EIS measurements are considerably lower than the *recorded* corrosion rates from the ER measurements.

Comparing the different electrochemical methods, the estimated corrosion rates from the EIS measurements are smaller than the ones obtained from the SmartCET® corrosion monitoring and the electrochemical frequency modulation technique, which is understandable due to the applied measuring frequency in the latter (the applied frequency is not low enough and overestimates the corrosion rate) (Rosborg et al. 2005). However, ignoring the absolute values all methods seem to replicate the *recorded* corrosion rates from the ER measurements.

Besides the data for the four ER sensors, Table 5-1a also includes data from SmartCET® corrosion monitoring on the pre-exposed and the new cylindrical copper electrodes in the bentonite test package. The former were emplaced in LOT test parcel A2 in the Äspö HRL in 1998 and the latter were installed in the bentonite test package in 2006 after retrieval from Äspö. Comparable rates have been obtained for the pre-exposed electrodes and somewhat lower values for the new copper electrodes.

The *recorded* corrosion rates from the ER measurements are compared to the *estimated* corrosion rates from the EIS measurements that best replicate the ER data in Figure 5-1. (Average values from Table 4-3 have been used.)

In summary, all methods yield low but measurable corrosion rates. However, most of the corrosion rates given in Table 5-1 are remarkably high compared to the gravimetrically estimated average corrosion rates for the copper coupons exposed in LOT test parcel A2 during six years, which were less than 0.5 µm/year. However, the EIS measurements yielded values of this magnitude.

Table 5-1a. *Recorded* corrosion rates from ER measurements compared with electrochemically measured corrosion rates in October 2008 and in April and November 2009 (in µm/year).

Sensor/electrode	ER			EIS			SmartCET®		EFM
	Oct-08	Apr-09	Nov-09	Oct-08	Apr-09	Nov-09	Oct-08	Nov-09	Apr-09
ER1	2.6	2.0	1.4	0.6–1.3	0.4–0.8	0.3–0.6	1.4–2.7		1.2–2.6
ER2							3.3–6.5		3.8–7.7
ER3	6.8	6.7	6.6				1.7–3.4		2.1–4.1
ER4	2.0	1.6	1.2	1.1–2.1	0.7–1.3	0.5–0.9	1.4–2.7		1.5–3.1
Pre-exposed							1.7–3.4	1.6–3.2	
New							0.7–1.4	0.5–1.1	

Table 5-1b. *Recorded* corrosion rates from ER measurements compared with electrochemically measured corrosion rates in 2010 and 2011 (in µm/year).

Sensor	ER			EIS		
	Nov-09	Feb-10	Mar-11	Nov-09	Feb-10	Mar-11
ER1	1.4	1.2	0.7	0.3–0.6	0.3–0.6	0.2–0.4
ER2						0.7–1.4
ER3	6.6	6.6				0.3–0.6
ER4	1.2	1.1	0.8	0.5–0.9	0.5–1.1	0.3–0.7

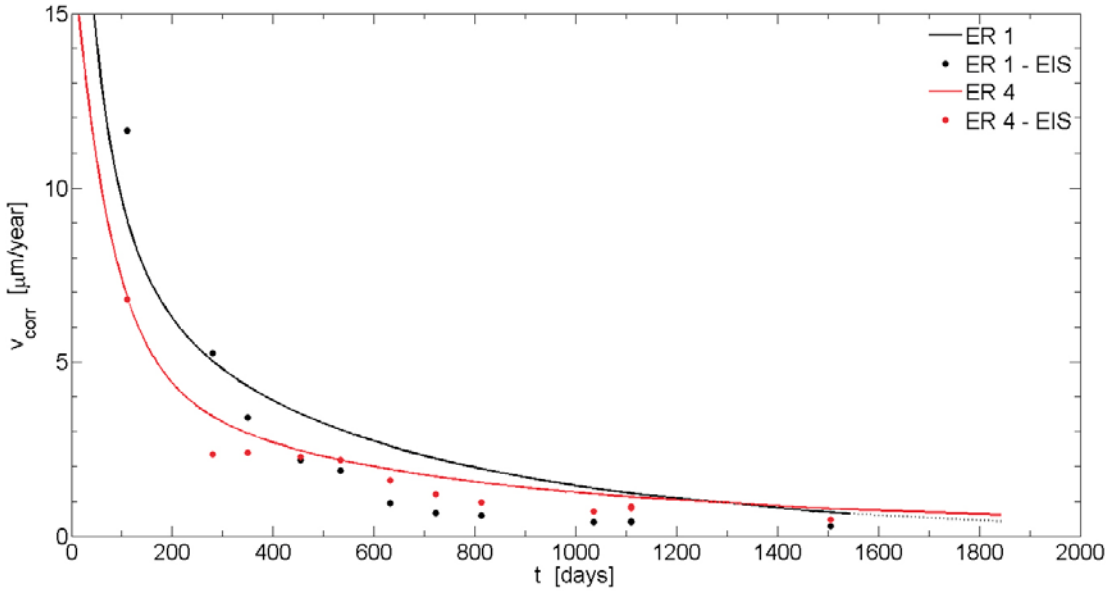

Figure 5-1. *Recorded corrosion rates for sensors ER1 and ER4 from the ER measurements (lines) compared to estimated corrosion rates from the EIS measurements (dots).*

5.3 Comparison of average corrosion rates

In Table 5-2 the average corrosion rates for the ER sensors in the bentonite test package, obtained from a comparison of cross-sections of corroded and non-corroded sensor elements, are compared with gravimetrically estimated average corrosion rates for copper coupons exposed in two LOT test parcels (Karnland et al. 2009, 2011). The table shows that the average corrosion rates of the ER sensors are comparable to the average corrosion rate of the copper coupon from LOT test parcel A0, but higher than for the copper coupons from LOT test parcel A2. Figure 4-12 shows clearly that a substantial part of the weight loss due to corrosion occurred quite early during exposure, and that the initial corrosion rate of the ER sensors varied considerably. The evolution of the environment next to the ER sensors at the start of exposure is crucial for the corrosion behaviour and estimated average corrosion rate. It is reasonable to anticipate that the corrosion potential of the copper coupons in LOT test parcel A2 (which has not been measured) was lower compared to the other samples in Table 5-2 (Rosborg 2013), which could have contributed to the lower average corrosion rate.

5.4 Real-time corrosion monitoring

Different approaches have been used to improve the understanding of copper corrosion under repository conditions, including thermodynamic considerations, field and laboratory testing, modelling of the corrosion behaviour, and examination of natural and archaeological analogues. The present work has demonstrated that real-time corrosion monitoring using electrochemical and ER techniques offers a further possibility. Real-time corrosion monitoring provides more informative data than mere exposure of copper coupons (Karnland et al. 2009, Rosborg 2013).

Table 5-2. Average corrosion rates for ER sensors in the oxic bentonite test package (btp – oxic) and comparable values for copper coupons from LOT test parcels A0 and A2.

Sample	Environment	Temp °C	Duration days	Corrosion potential mV (SHE)	Average corrosion rate µm/year
ER1	btp – oxic	RT	1,539	261	2.0
ER2	btp – oxic	RT	1,539	239	2.9
ER3	btp – oxic	RT	1,539	222	2.7
ER4	btp – oxic	RT	1,539	242	1.6
Coupon	LOT A0	35	710	–	3.4
Coupon	LOT A2	30	2,271	–	< 0.5

6 Conclusions

Four 35 µm thick ER sensors of pure copper were exposed to oxic conditions at room temperature in a bentonite test package during four years. The test package was made up from three bentonite rings that had been pre-exposed in the Äspö HRL to obtain a proper bentonite/saline groundwater environment. The corrosion potentials of the ER sensors in the bentonite package were in the range 222–261 mV (SHE) at the end of the exposure period.

Post-test examinations verified the presence of cuprite, Cu_2O, and paratacamite, $Cu_2(OH)_3Cl$, on the ER sensors after exposure and an uneven corrosion on the exposed sensor elements varying from only a slight attack to full penetration of the 35 µm thick electric lead.

Two out of the four ER sensors survived the entire test period of 1,539 days, while the other two failed within the test period. The cause of failure was localization of corrosion on the electric leads; one sensor failed in four months equivalent to a local average corrosion rate of about 90 µm/year; however, the average corrosion rate of the very same sensor was merely 2.9 µm/year.

The ER measurements have shown that the corrosion rate of pure copper exposed to an oxic bentonite/saline groundwater environment at room temperature decreases slowly with time to low but measurable values. The *recorded* corrosion rates of the ER sensors at start of exposure was higher than 15 µm/year but by the end of exposure was 0.7 and 0.8 µm/year for the two survivors. Based on the ER readings the average corrosion rate for the two survivors was 3.4 and 2.6 µm/year, respectively. The average corrosion rates estimated from a comparison of cross-sections on exposed and protected sensor elements were 2.0, 2.9, 2.7, and 1.6 µm/year for each sensor respectively. When comparing ER readings with an estimate of the average corrosion rate, it is noted that the former overestimates the corrosion rate, which is understandable considering the uneven corrosion attack on the sensors.

The corrosion rates estimated from the regularly performed electrochemical impedance spectroscopy measurements replicate the data obtained from the ER measurements, but are somewhat lower. Thus, electrochemical measurements with due consideration and correction for the applied measuring frequency give believable estimates of the actual corrosion rate for the present environmental conditions; for other redox conditions the situation could be different. It would appear that electrochemical measurements can provide a better estimate of the corrosion rate; however, this is quite dependent on the use of proper measuring frequencies and evaluation methods. In this respect ER measurements are more reliable.

In summary, the measurements have shown that the corrosion rate of pure copper exposed to an oxic bentonite/saline groundwater environment can be followed by both ER and electrochemical techniques, and that the corrosion rate decreases slowly with time to very low values (< 1 µm/year). The post-test examination of the four ER sensors after a test period of 1,539 days revealed cuprite and paratacamite as end corrosion products, uneven corrosion on the copper leads, and average corrosion rates below 3 µm/year similar to what has been found for copper coupons exposed in the LOT test parcels at Äspö.

References

SKB:s (Svensk Kärnbränslehantering AB) publications can be found at www.skb.se/publications.

ASTM G102 – 89(2010). Standard practice for calculation of corrosion rates and related information from electrochemical measurements. West Conshohocken, PA: ASTM International.

ASTM G96 – 90(2008). Standard guide for online monitoring of corrosion in plant equipment (Electrical and electrochemical methods). West Conshohocken, PA: ASTM International.

Betova I, Beverskog B, Bojinov M, Kinnunen P, Mäkelä K, Pettersson S-O, Saario T, 2003. Corrosion of copper in simulated nuclear waste repository conditions. Electrochemical Solid-State Letters 6, B19–B22.

Bosch R W, Bogaerts W F, 1996. Instantaneous corrosion rate measurement with small-amplitude potential intermodulation techniques. Corrosion 52, 204–212.

Bosch R W, Hubrecht J, Bogaerts W F, Syrett B, 2001. Electrochemical frequency modulation: A new electrochemical technique for online corrosion monitoring. Corrosion 57, 60–70.

Cottis R, Turgoose S, 1999. Electrochemical impedance and noise. Houston, TX: NACE International.

Darowicki K, J Majewska J, 1999. Harmonic analysis of electrochemical and corrosion systems – A review. Corrosion Reviews 17, 383–399.

Karnland O, Sandén T, Johannesson L-E, Eriksen T E, Jansson M, Wold S, Pedersen K, Motamedi M, Rosborg B, 2000. Long term test of buffer material. Final report on the pilot parcels. SKB TR-00-22, Svensk Kärnbränslehantering AB.

Karnland O, Olsson S, Nilsson U, 2006. Mineralogy and sealing properties of various bentonites and smectite-rich clay materials. SKB TR-06-30, Svensk Kärnbränslehantering AB.

Karnland O, Olsson S, Dueck A, Birgersson M, Nilsson U, Hernan-Håkansson T, Pedersen K, Nilsson Sara, Eriksen T E, Rosborg B, 2009. Long term test of buffer material at the ÄspöHard Rock Laboratory, LOT project. Final report on the A2 test parcel. SKB TR-09-29, Svensk Kärnbränslehantering AB.

Karnland O, Olsson S, Sandén T, Fälth B, Jansson M, Eriksen T E, Svärdström K, Rosborg B, Muurinen A, 2011. Long term test of buffer material at the Äspö HRL, LOT project. Final report on the A0 test parcel. SKB TR-09-31, Svensk Kärnbränslehantering AB.

Kear G, Barker B D, Walsh F C, 2004. Electrochemical corrosion of unalloyed copper in chloride media – a critical review. Corrosion Science 46, 109–135.

King F, Ahonen L, Taxén C, Vuorinen U, Werme L, 2001. Copper corrosion under expected conditions in a deep geological repository. SKB TR-01-23, Svensk Kärnbränslehantering AB.

King F, Kolar M, Maak P, 2008. Reactive-transport model for the prediction of the uniform corrosion behaviour of copper used fuel containers. Journal of Nuclear Materials 379, 133–141.

King F, Lilja C, Pedersen K, Pitkanen P, Vähänen M, 2010. An update of the state-of-the-art report on the corrosion of copper under expected conditions in a deep geologic repository. SKB TR-10-67, Svensk Kärnbränslehantering AB.

Kranjc A, 2012. Preliminary title: Corrosion rate measurements on copper using electrical resistance sensors. Master thesis. Jožef Stefan International Postgraduate School, Ljubljana, Slovenia.

Kuş E, Mansfeld F, 2006. An evaluation of the electrochemical frequency modulation (EFM) technique. Corrosion Science 48, 965–979.

Legat A, Kuhar V, 2008. Electric resistance probes. Patent SI 22559 A. Slovenian National Building and Civil Engineering Institute.

Litke C D, Ryan S R, King F, 1992. A mechanistic study of the uniform corrosion of copper in compacted clay-sand soil. AECL-10397, COG-91-304, Atomic Energy of Canada Limited.

Rendahl B, 1998. Avlägsnande av korrosionsprodukter på koppar (utkast II 98-08-18). KI Rapport 65 221, Korrosionsinstitutet (The Swedish Corrosion Institute). (In Swedish.)

Rosborg B, 2013. Post-test examination of a copper electrode from deposition hole 5 in the Prototype Repository. SKB R-13-14, Svensk Kärnbränslehantering AB.

Rosborg B, Pan J, 2008. An electrochemical impedance spectroscopy study of copper in a bentonite/saline groundwater environment. Electrochimica Acta 53, 7556–7564.

Rosborg B, Werme L, 2008. The Swedish nuclear waste program and the long-term corrosion behaviour of copper. Journal of Nuclear Materials 379, 142–153.

Rosborg B, Eden D, Karnland O, Pan J, Werme L, 2004. The corrosion rate of copper in a test parcel at the Äspö Hard Rock Laboratory. In Oversby V M, Werme L O (eds). Scientific basis for nuclear waste management XXVII: symposium held in Kalmar, Sweden, 15–19 June 2003. Warrendale, PA: Materials Research Society. (Materials Research Society Symposium Proceedings 807), 489–494.

Rosborg B, Pan J, Leygraf C, 2005. Tafel slopes used in monitoring of copper corrosion in a bentonite/groundwater environment. Corrosion Science 47, 3267–3279.

Rosborg B, Kosec T, Kranjc A, Pan J, Legat A, 2011a. Electrochemical impedance spectroscopy of pure copper exposed in bentonite under oxic conditions. Electrochimica Acta 56, 7862–7870.

Rosborg B, Kranjc A, Kuhar V, Legat A, 2011b. Corrosion rate of pure copper in an oxic bentonite/saline groundwater environment. Corrosion Engineering, Science and Technology 46, 148–152.

Scully J R, 2000. Polarization resistance method for determination of instantaneous corrosion rates. Corrosion 56, 199–217.

Stern M, Geary A L, 1957. Electrochemical polarization: I. A theoretical analysis of the shape of polarization curves. Journal of Electrochemical Society 104, 56–63.

Thompson N G, Payer J H , 1998. DC electrochemical test methods. Houston, TX: NACE International.

Trachli B, Keddam M, Takenouti H, Srhiri A, 2002. Protective effect of electropolymerized 3-amino 1,2,4-triazole towards corrosion of copper in 0.5 M NaCl. Corrosion Science 44, 997–1008.

Van Ingelgem Y, Hubin A, Vereecken J, 2007. Investigation of the first stages of the localized corrosion of pure copper combining EIS, FE-SEM and FE-AES. Electrochimica Acta 52, 7642–7650.

Werme L, 1998. Design premises for canister for spent nuclear fuel. SKB TR-98-08, Svensk Kärnbränslehantering AB.

Appendix A

Corrosion potential measurements

The corrosion potentials of the ER sensors have regularly been measured since May 2007.

Elucidation of the experimental procedure

Installation of reference electrodes – Two standard reference electrodes were installed in the bentonite test package just before covering the top of the test package with paraffin in January 2006. These were:

- one silver-silver chloride electrode (Radiometer REF 201, 537-11-028; 204 mV (SHE) at 20°C), and
- one calomel electrode (Radiometer REF 401 SCE, 325-13-018; 248 mV (SHE) at 20°C)

both with saturated potassium chloride solution in their reference solution compartments.

Two holes opposite to each other in the bentonite test package were first drilled into the bentonite. Perspex tubes with ceramic frits facing the bentonite/saline groundwater environment were placed in the holes. Some Äspö groundwater was poured into the Perspex tubes and constitutes the liquid junction. The reference electrodes were then placed inside the Perspex tubes. (The position of the reference electrodes in the bentonite test package is shown in Figure 3-1f in the main text.)

A measurement of the potential difference between the two reference electrodes has served as a functional test. The reference electrodes were positioned far from each other and a stable value between the electrodes has been used as verification that potential measurements were possible.

Instrumentation – Two Gamry Reference 600™ potentiostats (either REF600-04085 or REF600-11060) and the saturated silver-silver chloride reference electrode have been used for the potential measurements. On several occasions the corrosion potentials have been monitored over a 5 min period with a measuring frequency of one record per second. (These are marked with a file name in Table A-1 below.)

Applied procedure for potential measurements – As the bentonite with time "consumes" the liquid junction, Äspö groundwater has been used as liquid junction solution between the reference electrodes and the bentonite pore water. The groundwater is added to the Perspex tube after removal of the reference electrode, see below.

Thus, it is necessary to add new liquid junction solutions and the following procedure has been applied for a series of corrosion potential measurements:

- On several occasions the corrosion potentials of the copper samples and the potential difference between the two reference electrodes have been measured as arrived.[18]
- The reference electrodes have then been removed from the bentonite test package and examined for the presence of solid crystals in their reference solution compartments. If needed, solid potassium chloride crystals and reference solution have been added. New liquid junction solution in the form of a small quantity of Äspö groundwater has been added to the Perspex tube, and the reference electrodes have then been placed in the bentonite test package again and sealed with paraffin. No attempt has been made to deaerate the Äspö groundwater before addition.
- After a certain period, mostly over night, the potential difference between the reference electrodes has again been measured, and if a satisfactory value[19] has been obtained …
- … the corrosion potentials of all copper samples in the bentonite test package have been measured. From time to time files with the measured values over a 5 min period and a measuring frequency of one record per second have been stored.[20]

[18] It has been found that fairly good estimates of the corrosion potentials have been obtained without refurbishment of the liquid junction. The presence of a salt bridge between the tip of the reference electrode and the ceramic frit facing the bentonite is anticipated to be the reason for this.

[19] The measured potential difference was not far from the expected potential difference between the reference electrodes, that is 44 mV at 20°C.

[20] Part of this record has unfortunately been lost since one of the used PCs was stolen. However, written back-up values at the start of these measurements exist.

The applied procedure implies that a small quantity of Äspö groundwater has repetitively been added to the bentonite/saline groundwater environment. The groundwater was stored in plastic containers and no efforts have been made to deaerate the groundwater before addition. As a consequence a small quantity of oxygen has repetitively been added.

Measured corrosion potentials

Selected data from the recorded corrosion potentials are presented in Table A.1. The bentonite test parcel is kept at room temperature without any thermostatting, thus the temperature for the measurements has varied slightly as seen from the table.

Table A-1. Corrosion potentials of the ER sensors.

Date	Temp. °C	ER1 mV (SHE)	ER2 mV (SHE)	ER3 mV (SHE)	ER4 mV (SHE)	File	Note
2007-05-08	21.5	185	220	173	181	LOTA2.ERxa	Refurbished
2007-05-09	22.5	182	217	171	180		Ditto
2008-01-08	21.5	*210*	*219*	*205*	*216*		As arrived
2008-01-08	21.5	193	202	188	199		Refurbished
2008-01-09	21.5	193	201	187	199	LOTA2.ERxb	Ditto
2008-07-10	25	209	202	195	207		Refurbished
2008-10-22	23	210	204	202	213		Ditto
2009-02-23	22.5	*255*	*233*	*218*	*241*		As arrived
2009-02-24	23	240	218	202	226	LOTA2.ERxc	Refurbished
2009-03-11	22	*250*	*233*	*214*	*239*		As arrived
2009-03-12	22	237	221	202	227		Refurbished
2009-03-13	23.5	235	219	200	226	LOTA2.ERxd	Ditto
2009-04-15	22	*254*	*234*	*217*	*242*		As arrived
2009-04-17	23	239	219	206	228		Refurbished
2009-06-02	22	*259*	*208*	*221*	*247*		As arrived
2009-06-03	22	243	203	204	230	LOTA2.ERxe	Refurbished
2009-11-03	22	260	240	226	251		As arrived
2009-11-04	22.5	242	223	208	234	LOTA2.ERxf	Refurbished
2010-02-03	23.5	254	229	215	235		Refurbished
2010-03-08	22	*262*	*239*	*227*	*246*		As arrived
2010-04-26	19.5	262	236	223	241		Refurbished
2010-06-09	19.5	262	237	223	244		Refurbished
2010-06-12	19	260	234	221	241		Refurbished
2010-08-02	20.5	*265*	*245*	*228*	*247*		As arrived
2010-08-03	22	256	236	218	240		Refurbished
2010-09-08	19.5	275	254	242	258	LOTA2.ERxg	
2010-09-17	19	261	236	222	242		Refurbished
2010-10-04	19	261	238	223	243		Refurbished
2011-01-13	19.5	266	241	229	248		Refurbished
2011-02-11	21	263	236	225	243		Refurbished
2011-03-07	21.5	*277*	*254*	*237*	*257*		As arrived
2011-03-09	22	262	239	222	242		Refurbished
2011-03-14	21.5	268	246	229	248	LOTA2.ERxh	
2011-03-24	22	261	239	222	242		Refurbished
2011-04-11	21.5	271	249	233	250		

Note 1: As found from the table the “As arrived” values do not dramatically differ from the “Refurbished” values, that are the corrosion potentials measured after refurbishment of the reference electrode. Obviously galvanic contact still existed between the copper and reference electrodes also after the liquid junction had been “consumed” by the bentonite. It is anticipated that the galvanic contact was maintained by a salt bridge between the reference electrode tip and the pore water in the bentonite that caused a liquid junction potential of less than 20 mV.

Note 2: Files LOTA2.ERxy, where×is 1, 2, 3 or 4 and y is a, b, c, etc.

Appendix B

Recorded data from EIS measurements

Measurements

The performance of the EIS measurements is described in the main text. (For items 1 through 11 in Table 3-1 the REF600-04085 potentiostat and for item 12 the REF600-11060 potentiostat was used. The reference electrode was a Radiometer REF 401 SCE; 325-13-018; 248 mV (SHE) at 20°C.)

Evaluation procedures

Three ways of estimating the polarization resistance, R_p, have been applied.

R_p-values from |Z| at 1 mHz

The first way of estimating the polarization resistance was to simply and somewhat arbitrary take R_p as the absolute impedance |Z| at the smallest measured frequency (for the majority of measurements), that is at 1 mHz, and ignoring the electrolyte resistance since it is only a small fraction of the measured impedance. The R_p-values estimated from |Z| at 1 mHz are listed in Table B-1a below.

R_p-values from limited spectrum fitting

The polarization resistance can be obtained from fitting of the impedance data to equivalent circuits as described in (Cottis and Turgoose 1999)[21] and somewhat elaborated in the following.

The impedance spectrum for copper after short exposures in the bentonite/saline groundwater environment has earlier been found to be dominated by one relaxation (time constant) (Rosborg and Pan 2008). A simple equivalent circuit consisting of a polarization resistance R_p and an interfacial capacitance in parallel, connected in series with the electrolyte resistance R_s, can then be satisfactorily used for spectrum fitting. A constant-phase element (CPE) was used instead of a pure capacitance to account for a non-ideal capacitive response of the interface (Cottis and Turgoose 1999). The spectrum fitting to the simple circuit gave a R_p-value of 45 kohm·cm^2 after three days exposure.

However, this equivalent circuit is too simple to fully describe the impedance spectrum for copper after longer exposures in the bentonite/saline groundwater environment (Rosborg and Pan 2008). In several studies of copper in chloride solutions two or three time constants have been observed and different equivalent circuits used for data fitting (e.g. Van Ingelgem et al. 2007, Betova et al. 2003, Trachli et al. 2002). The equivalent circuits in Figure B-1 are generally used for impedance spectra fitting for copper exposed to saline solutions and mathematically very good fits can be obtained (Van Ingelgem et al. 2007). Different interpretations of the circuit elements exist and are briefly discussed in Van Ingelgem et al. (2007). In short, however, there is presently no consensus how to unambiguously interpret the different parameters obtained from spectra fitting and decide upon which physical model match the best.

For the present study a simplified spectrum fitting procedure was first applied using the ZView™ software program: the left equivalent circuit in Figure B.1 with two CPE:s and a frequency range from 10 kHz down to 0.099 Hz were chosen for the fitting. (Mathematically good fits were obtained with chi-square values in the range 0.0002 to 0.002 (Rosborg et al. 2011a).) The R_p-values were calculated as the sum of the partial resistances R_1 and R_2 in the equivalent circuit, that is $R_p = R_1 + R_2$. The estimated R_p-values from the limited spectrum fitting are listed in Table B-1b.

R_p-values from extended spectrum fitting

An equivalent circuit with two CPE:s (two time constants) could not describe the experimental data in the whole frequency range; thus, spectrum fitting using the equivalent circuit with three CPE:s (three time constants) in Figure B-1 was also applied. A frequency range from 10 kHz down to 1 mHz was used. (The chi-squares values varied from 0.0002 to 0.001.) The R_p values were again taken as the sum of the partial resistances R_1 and R_2 (and ignoring R_3 which may underestimate R_p, and thus overestimate the corrosion rate). The estimated Rp-values from the extended spectrum fitting are listed in Table B-1c.

For further information about the limited and extended spectrum fitting, see (Rosborg et al. 2011a).

[21] The references are listed in the main text.

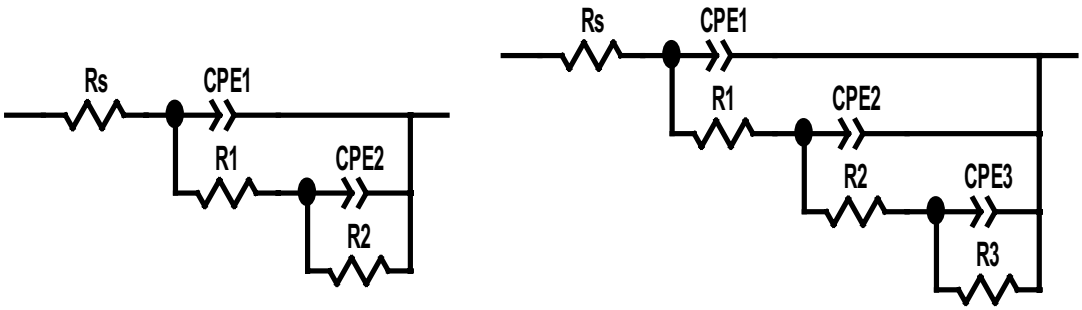

Figure B-1. *Proposed equivalent circuits for long exposures of copper in the bentonite/saline groundwater environment.*

Estimated corrosion rates

The estimated corrosion rates from the three evaluation procedures are listed in Tables B-2a through B-2c respectively. The corrosion rate is given as a range, with the lowest value representing a two-electron reaction (thus using n=2 in Faraday´s law) and the highest value representing a one-electron reaction (using n=1). A better estimate of the corrosion rate falls in between these values, since both univalent and divalent corrosion products have been formed, see section 4.6 in the main text.

In Figure B-2 the estimated corrosion rates from the electrochemical measurements are compared to the *recorded* corrosion rates from the ER measurements.

Comments

The EIS data replicates the ER data, in Figure B-2 exemplified by the corrosion rates obtained from the extended spectrum fitting, which fall closer to the ER data (ignoring R_3).

Table B-1a. Estimated R_p-values from |Z| at 1 mHz.

Date	Days of exposure	Polarization resistance in ohm·cm²			
		ER1	ER2	ER3	ER4
2007-01-23		*Installation of ER sensors*			
2007-05-14	**111**	22,099	42,820	72,569	109,767
2007-10-30	**280**	84,021		95,307	170,758
2008-01-08	**350**	119,098		111,222	204,519
2008-04-22	**455**	146,615		123,781	193,711
2008-07-09	**533**	163,688		135,387	214,116
2008-10-16	**632**	238,329		156,226	254,912
2009-01-14	**722**	334,432		197,589	327,348
2009-04-14	**812**	423,493	138,194	239,526	386,127
2009-11-24	**1,036**	583,177	129,202	295,505	479,598
2010-02-05	**1,109**	592,284			407,148
2010-02-06	**1,110**	577,724			434,945
2011-03-08	**1,505**	1,106 000	297,262	517,517	784,000

Table B-1b. Estimated R_p-values from limited spectrum fitting.

Date	Days of exposure	Polarization resistance in ohm·cm²			
		ER1	ER2	ER3	ER4
2007-01-23		*Installation of ER sensors*			
2007-05-14	**111**	53,424	55,377	79,842	102,781
2007-10-30	**280**	98,910		87,017	167,468
2008-01-08	**350**	115,710		110,719	199,122
2008-04-22	**455**	131,152		119,742	190,652
2008-07-09	**533**	131,082		131,355	203,154
2008-10-16	**632**	192,437		150,409	249,599
2009-01-14	**722**	238,721		206,990	317,135
2009-04-14	**812**	309,897	140,889	234,227	377,524
2009-11-24	**1,036**	615,069	132,601	286,748	513,331
2010-02-05	**1,109**	980,196			427,196
2010-02-06	**1,110**	921,669			445,067
2011-03-08	**1,505**	1,054 550	306,369	568,687	697,613

Table B-1c. Estimated R_p-values from extended spectrum fitting.

Date	Days of exposure	Polarization resistance in ohm·cm²			
		ER1	ER2	ER3	ER4
2007-01-23		*Installation of ER sensors*			
2007-05-14	**111**	22,442			38,227
2007-10-30	**280**	49,616			65,534
2008-01-08	**350**	77,175			107,429
2008-04-22	**455**	120,190			113,442
2008-07-09	**533**	137,564			118,762
2008-10-16	**632**	276,332			163,604
2009-01-14	**722**	392,343			215,873
2009-04-14	**812**	434,175			268,905
2009-11-24	**1,036**	627,984			370,132
2010-02-05	**1,109**	611,576			326,109
2010-02-06	**1,110**	614,600			305,746
2011-03-08	**1,505**	881,083	242,305	550,235	534,058

Table B-2a. Estimated corrosion rates from |Z| at 1 mHz (µm/year).

Date	Days of exposure	Recorded corrosion rates in µm/year			
		ER1	ER2	ER3	ER4
2007-01-23		*Installation of ER sensors*			
2007-05-14	**111**	8.1-16	4.1-8.1	2.4-4.8	1.6-3.2
2007-10-30	**280**	2.1-4.1		1.8-3.7	1.0-2.0
2008-01-08	**350**	1.5-2.9		1.6-3.1	0.85-1.70
2008-04-22	**455**	1.2-2.4		1.4-2.8	0.90-1.80
2008-07-09	**533**	1.1-2.1		1.3-2.57	0.81-1.63
2008-10-16	**632**	0.74-1.5		1.1-2.23	0.68-1.4
2009-01-14	**722**	0.52-1.1		0.88-1.9	0.53-1.06
2009-04-14	**812**	0.41-0.83	1.26-2.5	0.72-1.5	0.45-0.9
2009-11-24	**1,036**	0.3-0.6	1.35-2.7	0.59-1.2	0.36-0.73
2010-02-05	**1,109**	0.30-0.60			0.43-0.86
2010-02-06	**1,110**	0.30-0.60			0.40-0.80
2011-03-08	**1,505**	0.16-0.32	0.59-1.2	0.34-0.67	0.22-0.44

Table B-2b. Estimated corrosion rates from limited spectrum fitting.

Date	Days of exposure	Recorded corrosion rates in µm/year ER1	ER2	ER3	ER4
2007-01-23		*Installation of ER sensors*			
2007-05-14	**111**	3.3-6.5	3.1-6.3	2.2-4.4	1.7-3.4
2007-10-30	**280**	1.8-3.5		2.0-4.0	1.0-2.1
2008-01-08	**350**	1.5-3.0		1.6-3.1	0.88-1.75
2008-04-22	**455**	1.3-2.7		1.5-2.9	0.91-1.8
2008-07-09	**533**	1.3-2.7		1.3-2.65	0.86-1.7
2008-10-16	**632**	0.91-1.8		1.2-2.3	0.70-1.4
2009-01-14	**722**	0.73-1.46		0.84-1.68	0.55-1.1
2009-04-14	**812**	0.56-1.12	1.2-2.5	0.74-1.5	0.46-0.92
2009-11-24	**1,036**	0.28-0.57	1.3-2.6	0.61-1.2	0.33-0.67
2010-02-05	**1,109**	0.18-0.36			0.41-0.82
2010-02-06	**1,110**	0.19-0.38			0.39-0.78
2011-03-08	**1,505**	0.17-0.33	0.57-1.1	0.31-0.61	0.25-0.5

Table B-2c. Estimated corrosion rates from extended spectrum fitting.

Date	Days of exposure	Recorded corrosion rates in µm/year ER1	ER2	ER3	ER4
2007-01-23		*Installation of ER sensors*			
2007-05-14	**111**	7.8-15.5			4.5-9.1
2007-10-30	**280**	3.5-7.0			2.7-5.4
2008-01-08	**350**	2.3-4.5			1.6-3.2
2008-04-22	**455**	1.5-2.9			1.5-3.1
2008-07-09	**533**	1.3-2.5			1.5-2.9
2008-10-16	**632**	0.63-1.26			1.1-2.1
2009-01-14	**722**	0.44-0.89			0.81-1.6
2009-04-14	**812**	0.40-0.80			0.65-1.3
2009-11-24	**1,036**	0.28-0.55			0.47-0.94
2010-02-05	**1,109**	0.29-0.57			0.53-1.07
2010-02-06	**1,110**	0.28-0.56			0.57-1.14
2011-03-08	**1,505**	0.20-0.40	0.72-1.4	0.32-0.63	0.32-0.65

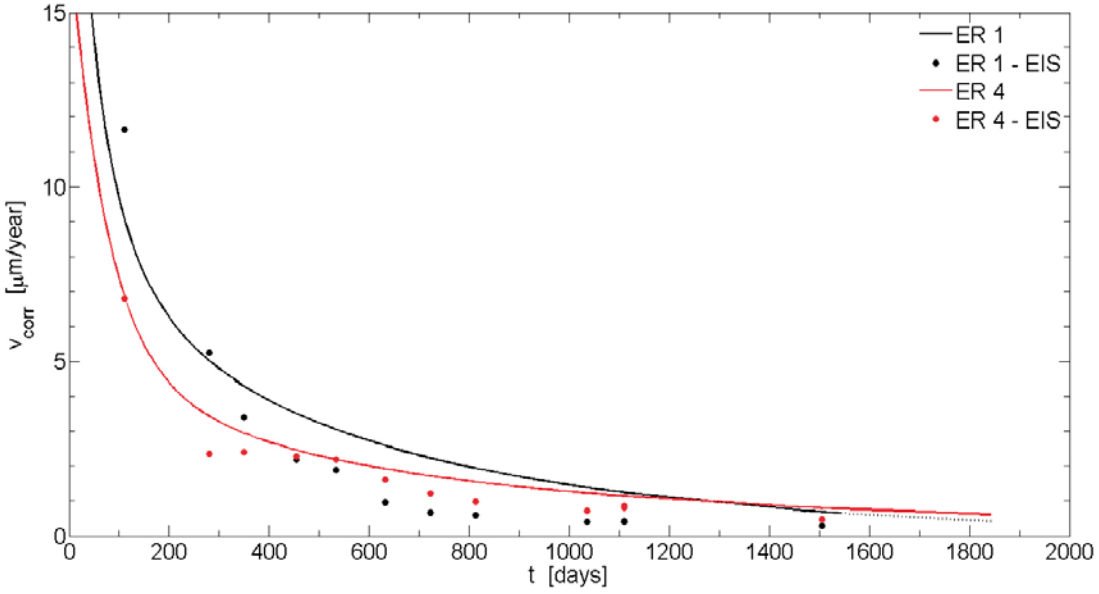

Figure B-2. *Recorded corrosion rates for sensors ER1 and ER4 from the ER measurements (lines) compared to estimated corrosion rates from the EIS measurements (dots).*

Appendix C

Recorded data from EFM measurements

So-called electrochemical frequency modulation (EFM) measurements have been applied on the ER sensors.

Further information about the EFM method

Information about the Electrochemical Frequency Modulation (EFM) technique can be obtained from the Gamry[22] website www.gamry.com. Here follows excerpts from the website information and the Gamry EFM140™ software manual (with slight modifications to shorten the text):

EFM is a harmonic technique that relies on the non-linear nature of the corrosion reaction to extract information about the corrosion rate and the Tafel constants. Two sinusoidal voltage waveforms are summed and applied to a corrosion sample. The resultant current response is recorded. The data is further transformed from the time domain into the frequency domain where the frequency response is analyzed to yield corrosion rate information.

The two frequencies may not be chosen at random. They must both be small, integer multiples of a 'base frequency' that determines the length of the experiment. The higher frequency must be at least two times the lower one. The higher frequency must also be sufficiently slow that the charging of the double layer does not contribute to the current response. Often, 10 Hz is a reasonable limit.

The result is a spectrum of current response as a function of frequency called the 'intermodulation spectrum'. The two large peaks are the response to the excitation frequencies. Smaller peaks are obtained for the harmonics, the sums, and the differences of the two excitation frequencies. These peaks are used by the EFM140™ software to calculate the corrosion current and the Tafel constants.

The EFM measurement also gives an internal self-check in the form of the two "Causality Factors". These two factors should have the values 2.0 and 3.0 if all of the conditions of EFM theory have been met.

Experimental

A Gamry Reference 600™ potentiostat (REF600-04085) and Gamry EFM140™ software were used for the three-electrode measurements. The nominal corroding surface area of the ER sensors is 7.0 cm^2. A saturated calomel electrode (Radiometer REF 401 SCE, 325-13-018; 248 mV (SHE) at 20°C) was used as reference electrode and the external copper sheet (with an electrode area > 1 dm^2) as counter electrode. The instrumental set-up for the single-shot EFM measurements[23] reported below was:

amplitude 10 mV

base frequency 1 mHz

multiplier A=2

multiplier B=5

4 cycles

n=1

With a base frequency of 1 mHz and multipliers of A=2 and B=5 the two applied sine waves had excitation frequencies of 2 and 5 mHz respectively.

The temperature was 22°C.

[22] Gamry Instruments, 734 Louis Drive, Warminster, PA 18974, US.

[23] as described in the Gamry EFM140™ software.

Recorded corrosion rates

Due to lack of prior experience with the method, a series of measurements using different amplitudes and base frequencies were first tried. Then a test series was performed with the above instrumental set-up and with the result given in the following table:

Table C-1. Recorded corrosion rates from single-shot EFM measurements.

Sensor	Date	Time	File	E_{corr} mV SHE	I_{corr} µA	Corrosion rate µm/year		Causality factors	
						n=1	n=2	2	3
ER1	2009-04-16	19:02	*EFMs.ER1d*	240	0.75	2.6	1.2	1.296	1.965
ER2	2009-04-16	20:37	*EFMs.ER2d*	219	2.32	7.7	3.8	1.931	2.946
ER3	2009-04-16	22:13	*EFMs.ER3d*	237	1.22	4.1	2.1	1.840	2.818
ER4	2009-04-17	09:39	*EFMs.ER4d*	229	0.92	3.1	1.5	1.375	1.514

The obtained causality factors deviate from the “target values” 2 and 3 respectively, see above. The sensors with the lowest corrosion rates deviate the most.

Appendix D

Recorded data from SmartCET® measurements

In October 2008 it was found that the corrosion potentials of the ER sensors were close to the potential of the saturated silver-silver chloride reference electrode, see Appendix A. Thus, it was possible to establish three-electrode configurations for SmartCET® corrosion monitoring with two ER sensors and the silver-silver chloride reference electrode[24]. The recorded data from these measurements are found below.

Experimental

The SmartCET® corrosion monitoring instrumentation applies a voltage perturbation with a frequency of 0.01 Hz and 50 mV peak-to-peak amplitude and measures and analyzes the current response synchronously with the perturbing sine wave. Polarization resistance and harmonic distortion analysis techniques are used to derive information regarding the general corrosion rate. The harmonic distortion analysis involves the measurement of the higher harmonic content at 0.02 and 0.03 Hz, which then allows for estimates of the anodic and cathodic Tafel coefficients and the Stern-Geary coefficient.

Three-electrode set-ups were established with one ER sensor acting as working (ERx), the silver-silver chloride electrode as reference (REF), and a second ER sensor as counter electrode (ERy). The second ER sensor was never taken from the same ER sensor pair for cell geometry considerations, but from the other pair. Thus, there are two sets of data for each ER sensor.

The SmartCET® Lab unit KTH with the following probe 1 settings was used:

default value of the Stern-Geary coefficient – B=10.3 mV

the atomic weight of copper – 63.54

50 ohm

electrode area – 12 cm^2; *since the actual electrode area was 7.0 cm^2 the recorded corrosion rates listed below have to be multiplied by 12/7*

density of pure copper – 8.94 g/cm^3

the number of electrons required to oxidize an atom – n=1

The temperature was 23°C.

Recorded corrosion rates

The read off primary data are shown in the table below, in which LPR=recorded corrosion rate from polarization resistance measurements with B=10.3 mV as default value, **Corrosion rate**=corrected corrosion rate from polarization resistance measurements according to LPR·B/10.3, **HDA**=recorded corrosion rate from harmonic distortion measurements, **B**=recorded Stern-Geary coefficient, β_a=exponential anodic Tafel coefficient, and β_c=exponential cathodic Tafel coefficient.

[24] The electrodes should have about the same electrode potentials.

ERx-REF-ERy Date/Time	LPR	Corrosion rate µm/year	HDA µm/year	B mV	Ba mV	Bc mV
ER1-REF-ER3						
2008-10-22 09:59	1.07	1.66	1.65	16	28	38
2008-10-22 10:06	1.06	1.54	1.50	15	25	34
2008-10-22 10:13	1.06	1.54	1.57	15	27	36
2008-10-22 10:20	1.06	1.54	1.55	15	26	35
2008-10-22 10:27	1.07	1.56	1.51	15	26	33
2008-10-22 14:24	1.11	1.62	1.62	15	26	36
2008-10-22 14:31	1.11	1.62	1.58	15	26	34
2008-10-22 14:38	1.11	1.62	1.62	15	26	35
ER1-REF-ER4						
2008-10-22 10:42	1.05	1.43	1.48	14	25	34
2008-10-22 10:49	1.06	1.44	1.46	14	25	33
2008-10-22 10:56	1.07	1.56	1.57	15	27	35
2008-10-22 11:03	1.06	1.44	1.47	14	25	32
2008-10-22 11:11	1.06	1.54	1.50	15	26	33
ER2-REF-ER3						
2008-10-22 12:08	2.85	3.60	3.64	13	25	28
2008-10-22 12:15	2.87	3.90	3.81	14	25	30
2008-10-22 12:22	2.85	3.87	3.89	14	26	30
2008-10-22 12:29	2.87	3.90	3.80	14	25	30
2008-10-22 12:37	2.85	3.87	3.88	14	26	30
ER2-REF-ER4						
2008-10-22 11:25	2.82	3.56	3.60	13	24	28
2008-10-22 11:32	2.84	3.58	3.64	13	25	29
2008-10-22 11:39	2.84	3.58	3.66	13	25	29
2008-10-22 11:46	2.84	3.58	3.59	13	24	28
2008-10-22 11:54	2.85	3.60	3.68	13	25	29
ER3-REF-ER1						
2008-10-21 23:28	1.37	1.86	1.83	14	25	30
2008-10-21 23:35	1.37	2.00	1.95	15	27	32
2008-10-21 23:42	1.38	1.88	1.88	14	26	31
2008-10-21 23:49	1.38	1.88	1.93	14	26	32
2008-10-21 23:57	1.38	1.88	1.93	14	26	32
ER3-REF-ER2						
2008-10-22 09:23	1.50	2.18	2.21	15	29	33
2008-10-22 09:30	1.49	2.31	2.27	16	29	34
2008-10-22 09:37	1.49	2.17	2.19	15	28	33
ER4-REF-ER1						
2008-10-21 22:45	1.04	1.72	1.69	17	27	43
2008-10-21 22:52	1.04	1.72	1.74	17	28	45
2008-10-21 22:59	1.04	1.82	1.77	18	28	46
2008-10-21 23:06	1.05	1.83	1.80	18	29	46
2008-10-21 23:14	1.03	1.80	1.82	18	29	48
ER4-REF-ER2						
2008-10-21 21:55	1.10	1.39	1.43	13	24	30
2008-10-21 22:02	1.11	1.51	1.51	14	25	31
2008-10-21 22:16	1.09	1.48	1.43	14	25	30
2008-10-21 22:23	1.09	1.38	1.40	13	24	29
2008-10-21 22:31	1.09	1.38	1.42	13	24	30

Appendix E

Cross-sections of ER sensors

The cross-sections of the electric leads in the corroded and protected (reference) sensor elements from the very same ER sensor have been measured. Each ER sensor contains four sensor elements, see Paragraph 3.2.1 in the main text, and a plane through each sensor element contains 18 cross-sections of the electric lead.

The areas of the cross-sections were measured in the following way: The specimens were cut, grinded and polished with 1 µm polycrystalline diamond suspension, and then pictured on a Carl Zeiss AXIO Imager M2z metallographic microscope equipped with AXIO VISION 9/2009 software. The areas of the cross-sections were measured with image analysis using Multiphase software. (Due to sampling for other purposes a few of the lead parts were not available for measurements.)

The following tables give the results from the measurements.

Sensor ER1

Table E-1a summarizes the areas of cross-sections for the electric leads in sensor ER1. Sensor elements A1 and A2 are corroded and sensor elements A3 and A4 were protected. Table E.1b presents the distribution of the measured areas in percentage of the average area of the protected sensor elements.

Localization of the corrosion attack has almost resulted in penetration of the electric lead at one location, that is in sensor element A2 part g.

Sensor ER2

Tables E-2a and E-2b summarizes ditto for sensor ER2. Sensor elements B1 and B2 are corroded and sensor elements B3 and B4 were protected.

Localization of the corrosion attack has penetrated the electric lead in sensor element B2 at two locations, that is in parts j and k. It is obvious from Table E-2b that the corrosion on sensor ER2 is more uneven compared to sensor ER1.

Sensor ER3

Tables E-3a and E-3b summarizes ditto for sensor ER3. The corrosion attack on sensor element C1 is very uneven compared to sensor element C2.

Sensor ER4

Tables E-4a and E-4b summarizes ditto for sensor ER4.

Table E-1a. Areas of cross-sections for the electric leads in sensor ER1 (mm^2).

Part[1]	Sensor element/Cross-section						
	A1			A2		A3	A4
	1	2	3	1	2	1	1
a	0.0177	0.0151	0.0139	0.0159	0.0097	0.0220	0.0218
b	0.0194	0.0203	0.0194	0.0138	0.0128	0.0207	0.0219
c	0.0198	0.0187	0.0194	0.0139	0.0126	0.0213	0.0212
d	0.0184	0.0172	0.0182	0.0131	0.0157	0.0211	0.0217
e	0.0201	0.0178	0.0133	0.0130	0.0148	0.0209	0.0211
f	0.0192	0.0182	0.0186	0.0142	0.0149	0.0216	0.0225
g	0.0191	0.0158	0.0142	0.0043	0.0143	0.0215	0.0217
h	0.0173	0.0192	0.0171	0.0136	0.0207	0.0206	0.0204
l	0.0199	0.0169	0.0154	0.0142	0.0203	0.0212	0.0223
j	0.0192	0.0200	0.0179	0.0181	0.0193	0.0207	0.0221

Part[1]	Sensor element/Cross-section						
	A1		A2			A3	A4
k	0.0138	0.0181	0.0200	0.0112	0.0161	0.0208	0.0219
l	0.0153	0.0178	0.0133	0.0130	0.0142	0.0217	0.0215
m	0.0171	0.0162	0.0161	0.0152	0.0160	0.0210	0.0228
n		0.0172	0.0144	0.0158	0.0133	0.0208	0.0215
o				0.0167	0.0181	0.0222	0.0222
p				0.0165	0.0205	0.0217	0.0213
r		0.0201		0.0148	0.0176	0.0216	0.0214
s		0.0213		0.0157	0.0160	0.0213	0.0209
Interval			0.0043 – 0.0213			0.0204 – 0.0228	
Average			**0.0164**			**0.0215**	

[1] The letter q is not used in the Slovenian language and is thus missing.

Table E-1b. Distribution of areas of cross-sections for sensor ER1.

	Sensor element			
	A1	A2	A3	A4
0–10				
10–20		1		
20–30				
30–40				
40–50		1		
50–60		17		
60–70	6	11		
70–80	11	6		
80–90	15	3		
> 90	11	3	18	18
Items	43	36	18	18

Table E-2a. Areas of cross-sections for the electric leads in sensor ER2 (mm^2).

Part	Sensor element/Cross-section					
	B1		B2	B3	B4	
	1	2		1	2	1	2
a	0.0087			0.0230	0.0224	0.0224	0.0225
b	0.0123	0.0192		0.0229	0.0234	0.0231	0.0225
c	0.0155	0.0121		0.0226	0.0235	0.0211	0.0218
d	0.0129	0.0140		0.0228	0.0227	0.0216	0.0219
e	0.0164	0.0132		0.0230	0.0226	0.0226	0.0224
f	0.0179	0.0066		0.0221	0.0226	0.0227	0.0230
g	0.0216	0.0141		0.0226	0.0226	0.0217	0.0230
h	0.0219	0.0133		0.0225	0.0215	0.0184	0.0227
l	0.0172	0.0011		0.0225	0.0224	0.0212	0.0223
j	0.0162	0		0.0216	0.0216	0.0192	0.0209
k	0.0164	0		0.0220	0.0224	0.0212	0.0205
l	0.0155	0.0038		0.0219	0.0228	0.0219	0.0213
m	0.0171	0.0140		0.0227	0.0222	0.0219	0.0212
n	0.0152	0.0158		0.0219	0.0223	0.0217	0.0214
o	0.0180	0.0212		0.0234	0.0215	0.0210	0.0220
p	0.0189	0.0193		0.0230	0.0215	0.0220	0.0230
r	0.0185	0.0216		0.0222	0.0212	0.0208	0.0216
s	0.0195	0.0156		0.0227	0.0220	0.0220	0.0217
Interval		0 – 0.0219			0.0184 – 0.0235		
Average		**0.0144**			**0.0221**		

Table E-2b. Distribution of areas of cross-sections for sensor ER2.

	Sensor element		
	B1	**B3**	**B4**
0–10	3		
10–20	1		
20–30	1		
30–40	1		
40–50			
50–60	4		
60–70	5		
70–80	9		
80–90	7		2
> 90	4	36	34
Items	35	36	36

Table E-3a. Areas of cross-sections for the electric leads in sensor ER3 (mm^2).

Part	**Sensor element/Cross-section**										
	C1					**C2**				**C3**	**C4**
	1–1	1–2	2	3	4	1	2	3	4	1	1
a	0.0183	0.0157	0.0136	0.0144	0.0188	0.0219	0.0146	0.0136	0.0180	0.0248	0.0234
b	0.0204	0.0128	0.0168	0.0182	0.0221	0.0164	0.0121	0.0148	0.0195	0.0251	0.0246
c	0.0050	0.0151	0.0137	0.0197	0.0226	0.0156	0.0206	0.0139	0.0172	0.0252	0.0246
d	0.0059	0.0019	0.0222	0.0165	0.0223	0.0180	0.0188	0.0134	0.0193	0.0254	0.0246
e	0.0048	0.0028	0.0183	0.0167	0.0191	0.0214	0.0149	0.0154	0.0195	0.0253	0.0244
f	0.0083	0.0038	0.0147	0.0161	0.0225	0.0154	0.0219	0.0169	0.0202	0.0250	0.0252
g	0.0186	0.0130	0.0129	0.0146	0.0194	0.0168	0.0169	0.0190	0.0200	0.0255	0.0248
h	0.0216	0.0157	0.0132	0.0145	0.0230	0.0211	0.0219	0.0122	0.0205	0.0255	0.0251
l	0.0206	0.0139	0.0165	0.0140	0.0223	0.0215	0.0223	0.0200	0.0216	0.0249	0.0248
j	0.0192	0.0179	0.0158	0.0122	0.0219	0.0216	0.0204	0.0165	0.0194	0.0259	0.0249
k	0.0247	0.0189	0.0214	0.0144	0.0210	0.0183	0.0219	0.0140	0.0216	0.0258	0.0251
l	0.0196	0.0173	0.0129	0.0130	0.0223	0.0177	0.0133	0.0186	0.0219	0.0260	0.0253
m	0.0157	0.0145	0.0195	0.0212	0.0180	0.0204	0.0187	0.0180	0.0209	0.0248	0.0251
n	0.0130	0.0133	0.0164	0.0208	0.0158	0.0205	0.0134	0.0194	0.0204	0.0246	0.0247
o	0.0232	0.0165	0.0127	0.0194	0.0133	0.0179	0.0199	0.0208	0.0193	0.0249	0.0249
p	0.0236	0.0199	0.0145	0.0193	0.0143	0.0113	0.0144	0.0148	0.0170	0.0254	0.0248
r	0.0158	0.0119	0.0133	0.0213	0.0170	0.0108	0.0166	0.0114	0.0183	0.0242	0.0239
s	0.0148	0.0125	0.0119	0.0127	0.0172	0.0130	0.0168	0.0154	0.0162	0.0246	0.0255
Interval	0.0019 – 0.0247									0.0234 – 0.0260	
Average	**0.0169**									**0.0250**	

Table E-3b. Distribution of areas of cross-sections for sensor ER3.

	Sensor element			
	C1	**C2**	**C3**	**C4**
0–10	1			
10–20	4			
20–30	1			
30–40	1			
40–50	4	5		
50–60	25	12		
60–70	16	14		
70–80	18	20		
80–90	15	21		
> 90	5		18	18
Items	90	72	18	18

Table E-4a. Areas of cross-sections for the electric leads in sensor ER4 (mm^2).

Part	Sensor element/Cross-section							
	D1			D2			D3	D4
	1	3	4	1	2	3	1	1
a	0.0185	0.0152	0.0155	0.0139	0.0142	0.0157	0.0224	0.0223
b	0.0144	0.0160	0.0200	0.0212	0.0140	0.0208	0.0226	0.0228
c	0.0216	0.0199	0.0209	0.0188	0.0200	0.0203	0.0229	0.0225
d	0.0145	0.0153	0.0145	0.0201	0.0199	0.0182	0.0232	0.0224
e	0.0246	0.0134	0.0120	0.0212	0.0199	0.0160	0.0234	0.0226
f	0.0226	0.0168	0.0197	0.0203	0.0168	0.0127	0.0231	0.0224
g	0.0190	0.0219	0.0090	0.0203	0.0187	0.0187	0.0238	0.0227
h	0.0205	0.0177	0.0140	0.0198	0.0165	0.0197	0.0234	0.0227
I	0.0228	0.0142	0.0150	0.0216	0.0146	0.0197	0.0232	0.0221
j	0.0207	0.0145	0.0201	0.0210	0.0196	0.0209	0.0222	0.0228
k	0.0222	0.0111	0.0200	0.0191	0.0194	0.0201	0.0229	0.0227
l	0.0228	0.0132	0.0116	0.0199	0.0201	0.0201	0.0233	0.0219
m	0.0158	0.0212	0.0149	0.0206	0.0203	0.0130	0.0232	0.0222
n	0.0219	0.0219	0.0166	0.0206	0.0204	0.0166	0.0226	0.0231
o	0.0209	0.0184	0.0197	0.0197	0.0196	0.0199	0.0230	0.0216
p	0.0214	0.0207	0.0172	0.0197	0.0123	0.0191	0.0220	0.0217
r	0.0213	0.0217	0.0208	0.0171	0.0105	0.0182	0.0219	0.0216
s	0.0211	0.0214	0.0122	0.0196	0.0131	0.0184	0.0215	0.0220
Interval	0.0090 – 0.0246						0.0216 – 0.0238	
Average	**0.0182**						**0.0226**	

Table E-4b. Distribution of areas of cross-sections for sensor ER4.

	Sensor element			
	D1	D2	D3	D4
0–10				
10–20				
20–30				
30–40	1			
40–50	1	1		
50–60	5	4		
60–70	12	5		
70–80	5	5		
80–90	9	30		
> 90	21	9	18	18
Items	54	54	18	18